DEPARTMENT OF THE INTERIOR
U.S. GEOLOGICAL SURVEY

THERMAL MATURITY AND ORGANIC GEOCHEMISTRY OF THE KANDIK BASIN REGION, EAST-CENTRAL ALASKA

by

M.B. Underwood[1,2], M.M. Laughland[2], T.J. Wiley[1], and D.G. Howell[1]

Open-File Report 89-353

Prepared in cooperation with the University of Missouri, Columbia

[1] U.S. Geological Survey
Menlo Park, CA

[2] Department of Geology
University of Missouri
Columbia, MO

1989

TABLE OF CONTENTS

LIST OF FIGURES

LIST OF TABLES

ABSTRACT

The Kandik basin region straddles the border between the United States and Canada in east-central Alaska. The Tintina fault, a prominent right-lateral northwest-trending fault, marks the southwest limit of the study area. Basinal strata are divided by the northeast-trending Glenn Creek fault system. Strata northwest of the fault zone (Kandik River block) are Permian to latest Early Cretaceous (Albian) in age, whereas the southeast block (Nation River block) contains a sequence that is Late Proterozoic through Triassic or Jurassic in age.

Rock-Eval pyrolysis indicates that Type III and Type IV kerogens predominate throughout the study area; contents of total organic carbon range from 0.15 wt-% to 5.26 wt-%. Measurements of mean vitrinite reflectance (R_m) and illite crystallinity (CI) demonstrate that the Kandik River block reached significantly higher levels of thermal maturity than the Nation River block. R_m for Mesozoic shales northwest of the Glenn Creek fault ranges from 1.6% to 4.2%. With the exception of one anomalous sample, values for Paleozoic samples southeast of the fault range between only 0.6% and 1.2%R_m. There is a significant linear correlation between R_m and CI, which confirms the crude inversion of metamorphic grade with respect to stratal age.

Using time-independent methods for converting R_m to peak paleotemperature, we estimate contrasts across the Glenn Creek fault system of at least 100°C, and maximum variations are as high as 200-250°C. The stratal overburden required for this magnitude of heating during Cretaceous time remains unidentified, as does the mechanism of subsequent uplift. Thus, even though past workers have drawn stratigraphic correlations between the two fault blocks, their respective thermal histories are definitely allochthonous.

ACKNOWLEDGEMENTS

This work was partially funded by USGS/DOE interagency agreement DE-A121-83-MC20422 as part of the DOE Deep Source Gas program. D.L. Jones, P.J. Coney, R.W. Murray, S. Boundy-Sanders, and the late L. Kauffman-Linam provided valuable contributions to the field work. G. Wood, S.M. Kang, and A. Moreau assisted in the laboratory at the University of Missouri. Rock-Eval pyrolysis was completed by T.A. Daws. Les Magoon reviewed the manuscript.

INTRODUCTION

The Kandik area is located along the border between Alaska and Canada near latitude 65°N [Figure 1]. The stratigraphic section includes rocks ranging in age from Late Precambrian to early Tertiary. The lithologies, biostratigraphy, structural geology, and tectonic evolution of this region have been summarized recently by Howell and Wiley (1987). The purpose of this report is to provide complimentary information concerning thermal maturity, organic geochemistry, and petroleum source-bed potential.

Stratigraphy

The basic stratigraphic and structural relations of the Kandik area were mapped previously by Green and Roddick (1961), Brabb and Churkin (1969), Foster (1976), Norris (1979), and Dover and Miyaoka (1988). Figure 2 shows the generalized geology and a stratigraphic column. Stratal units analyzed during our laboratory study include the Tindir Group (Precambrian), the Funnel Creek Limestone (Cambrian), the Road River Formation (Ordovician-Devonian), the McCann Hill Chert (Devonian), the Nation River Formation (Devonian), the Ford Lake Shale (Devonian-Mississippian), the Glenn Shale (Triassic-Cretaceous), the Biederman Argillite (Cretaceous), and the Kathul Graywacke (Cretaceous) [see Table 1 for geologic summaries of these units].

Structural Geology

There are several regional-scale folds and faults in the Kandik area. The Tintina fault, which is a major right-slip fault, forms the southwest limit of Kandik basin. Thrust faults within the basin and along the basin margins strike east to northeast, and the axes of megascopic folds trend in that same general direction [Figure 2]. The most important structural feature with respect to thermal-maturity trends is the Glenn Creek fault zone [Figure 2]. This complex system of faults is roughly parallel to the "Glenn Creek fault", which was mapped by Brabb and Churkin (1969) as a high-angle fault with down-to-the-north displacement. Recent interpretations by Dover (1985) suggest that a dominantly-Mesozoic section to the northwest has been thrust towards the southeast over a dominantly-Paleozoic section, and Dover and Miyaoka (1988) refer to the fault zone as the Kandik Detachment. Howell and Wiley (1987) discussed the possibility of a southeast-dipping thrust. Diagnostic kinematic indicators of fault displacement have not been described or measured.

Tectonostratigraphy

Because of the fundamental uncertainties regarding both fault orientation and vergence, we simply use non-genetic terminology for the northwest block (**Kandik River block**) and the southeast block (**Nation River block**) of the Glenn Creek fault system. At this stage of the investigation, we have not identified formal *tectonostratigraphic terranes*, though ongoing (and more comprehensive) studies by Wiley should result in reliable genetic designations of that type.

Structural complexities make the fault-block assignment uncertain for strata in the northeast portion of the study area [see Figure 2]. Based upon stratigraphic affinities, however, those Cretaceous rocks are tentatively included in the Kandik River block. The Glenn Shale is also a problematic unit because the largely unfossiliferous mudrocks crop out in both fault blocks and span an age range of Triassic to Early Cretaceous. Brabb (1969) recognized that Triassic fossils are seemingly restricted to southern exposures of the formation, and Cretaceous fossils have been found only in northern exposures. Consequently, we tentatively divide the Glenn Shale into a

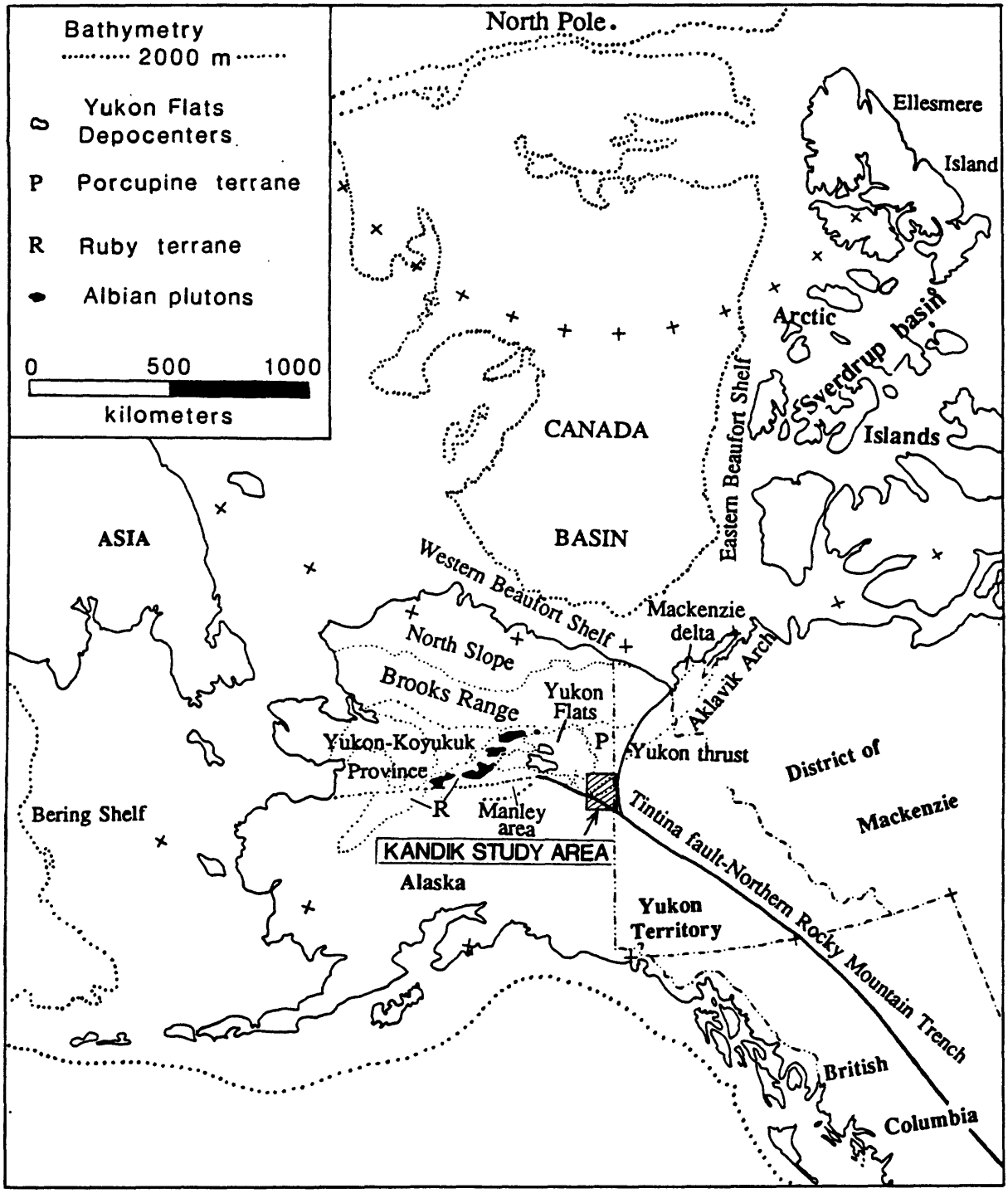

Figure 1. Index map showing the location of the Kandik basin study area.

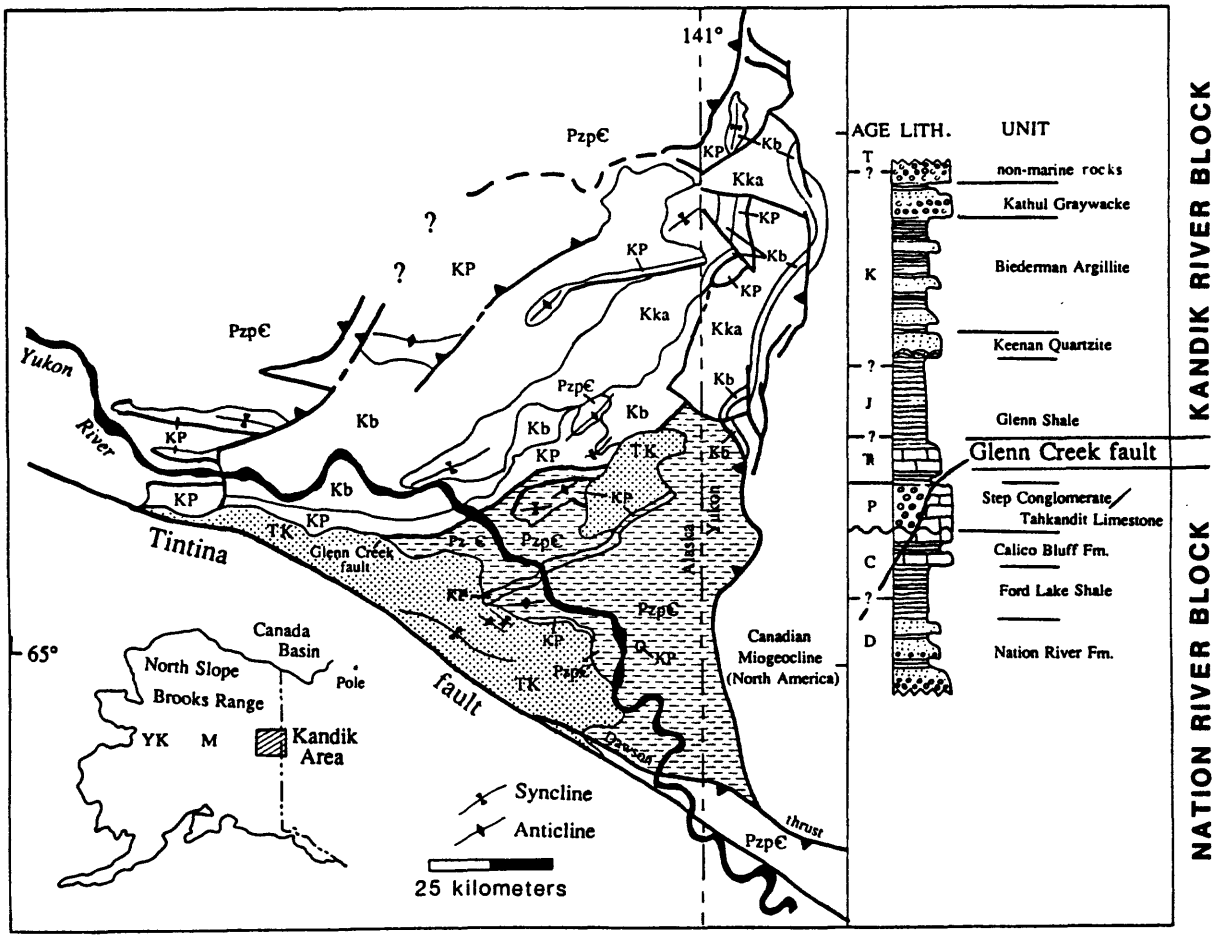

Figure 2. Generalized geology and stratigraphic column for the Kandik basin study area. Map unit symbols are as follows: TK (stippled pattern), non-marine Tertiary and Cretaceous rocks; Kka, Kathul Graywacke; Kb, Biederman Argillite; KP, undifferentiated Cretaceous to Permian rocks (Keenan Quartzite, Glenn Shale, Step Conglomerate, and Tahkandit Limestone); PzpC, undifferentiated Paleozoic and Precambrian rocks (Calico Bluff Formation, Ford Lake Shale, Nation River Formation, and Tindir Group). Nation River block is highlighted by hatchured pattern. Modified from Howell and Wiley (1987).

TABLE 1. Stratigraphic Units Sampled for Geochemical Analyses, Kandik Basin Region, Alaska

Stratigraphic Unit	Symbol	Age	Lithology/*Facies*
Kandik Group	K_{kg}	E.Cretaceous	undifferentiated Kka + Kb *deep-marine turbidites*
Kathul Graywacke	K_{ka}	Albian (?)	sandstone-conglomerate *deep-marine turbidites*
Biederman Argillite	K_b	Valanginian	sandstone-shale *deep-marine turbidites*
Glenn Shale	KTr_g	Triassic-E. Cretaceous	black shale-siltstone *deep marine*
Ford Lake Shale	MD_f	L. Devonian-Mississippian	siliceous shale-chert *deep marine*
Nation River Fm.	D_{nr}	Devonian	mudstone-sandstone-congl. *submarine fan complex*
McCann Hill Chert	D_m	Devonian	chert-siliceous shale *deep marine/pelagic*
Road River Fm.	DOS_r	E. Ordovician-E. Devonian	black shale-chert *slope to basin plain*
Funnel Creek Lms.	C_f	Cambrian	limestone-dolomite *paralic to slope*
Tindir Group	pC_t	Proterozoic	mainly dolomite-shale *continental breakup/glacial*

Triassic-Jurassic section (assigned to the Nation River block) and a Jurassic-Cretaceous section (assigned to the Kandik River block).

Undifferentiated non-marine sequences of Cretaceous (?) to Tertiary age rest unconformably above both fault blocks and cover significant portions of the main fault trace [Figure 2]. The lower age limit on these cover sequences is uncertain, but the sandstones and conglomerates may be as old as Albian (Brabb, 1969; Brabb and Churkin, 1969). Age diagnostic fossils are also lacking for the youngest marine sequences that can be assigned with certainty to the Kandik River block (Kathul Graywacke); however, quartzites within the apparent northeast extension of the Kandik River block [Figure 2] contain *Glycimeris* megafossils of probable Albian age (Jack Miller, personal communication, 1988). Furthermore, lithologic similarities and considerations of detrital provenance support a possible correlation between the Kathul Graywacke and early Albian nonmarine strata that crop out in the Eagle D1 quadrangle farther to the southeast (Howell and Wiley, 1987). If these stratigraphic correlations are correct, then the timing of displacement along the Glenn Creek fault system must be restricted to middle to late Albian time.

METHODS

All of the samples analyzed during this study were collected from fresh appearing surface exposures. Analytical methods included vitrinite reflectance, X-ray diffraction for illite crystallinity, and Rock-Eval pyrolysis. General descriptions of these methods, as well as conventional applications of the resulting data, have been outlined by Dow (1977), Bostick (1979), Kisch (1980), Dow and O'Connor (1982), Stach et al. (1982), and Peters (1986).

Vitrinite Reflectance

The procedures followed at the University of Missouri for vitrinite sample preparation and data acquisition are the same as those described in other Open-File Reports (Underwood and O'Leary, 1985; Underwood and Strong, 1986a). Briefly, kerogen was first concentrated using acid maceration methods, then mixed with epoxy on glass slides, polished, immersed in oil (RI = 1.5180), and measured under a stable reflected light source using a digital photometer. Values of mean reflectance (**Rm**) are calculated following measurements in oil (**Ro**) of approximately 50 randomly-oriented particles per sample. Past comparisons between UMC data and results from two commercial laboratories indicate that the accuracy of the technique is better than $\pm$0.1%Rm over relatively low levels of thermal maturity (<1.5%Rm). A higher degree of interlaboratory variability has been reported by Dembicki (1984), however, especially with higher-grade rocks. This increased scatter is partially because of analytical technique, but also because the amount of reflectance anisotropy (or bireflectance) increases as a function of organic metamorphism (Frey et al., 1980; Stach et al., 1982); this, in turn, raises the value of standard deviation for any given value of mean reflectance [Figure 3]. Bireflectance is also influenced by tectonic structures (Stone and Cook, 1979; Hower and Davis, 1981; Levine and Davis, 1984).

Reflectance data obtained from randomly-oriented dispersed particles are routinely plotted on histograms to test for abnormal statistical distributions. Many organic petrographers regard the higher modes in a polymodal reflectance population as indicative of recycled vitrinite particles (e.g., Dow and O'Connor, 1982). However, the well-documented rise in bireflectance with increasing coal rank means that the first mode (alone) on a reflectance histogram does not always represent the "indigenous" thermal maturity. Consequently, we have adopted a more conservative approach to the statistical treatment of polymodal patterns and suspected recycled grains. First, a value of mean reflectance is calculated using all measured particles. This number is then used to determine the acceptable "window" of reflectance anisotropy (i.e., R_{mean} versus R_{max}), based upon

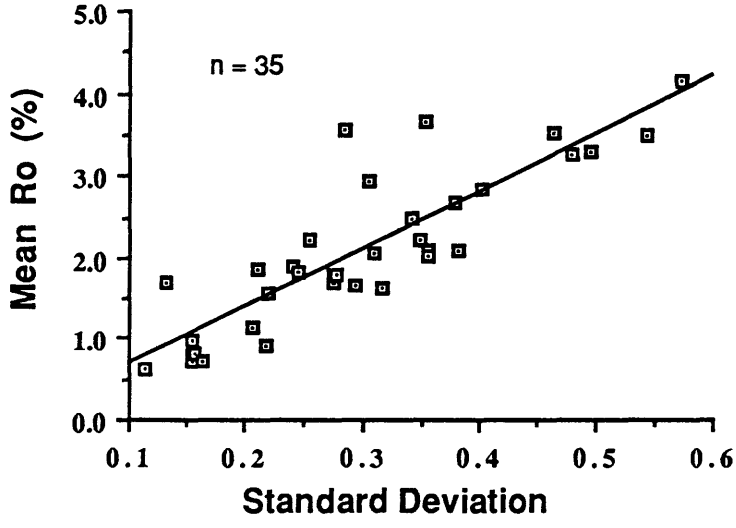

Figure 3. Linear regression plot showing the correlation between mean vitrinite reflectance and standard deviation. This relationship is caused largely by the progressive increase in bireflectance (or reflectance anisotropy) with increasing rank of organic metamorphism (see Figure 4 below). All data were obtained from Ordovician through Cretaceous strata of the Kandik basin region, Alaska.

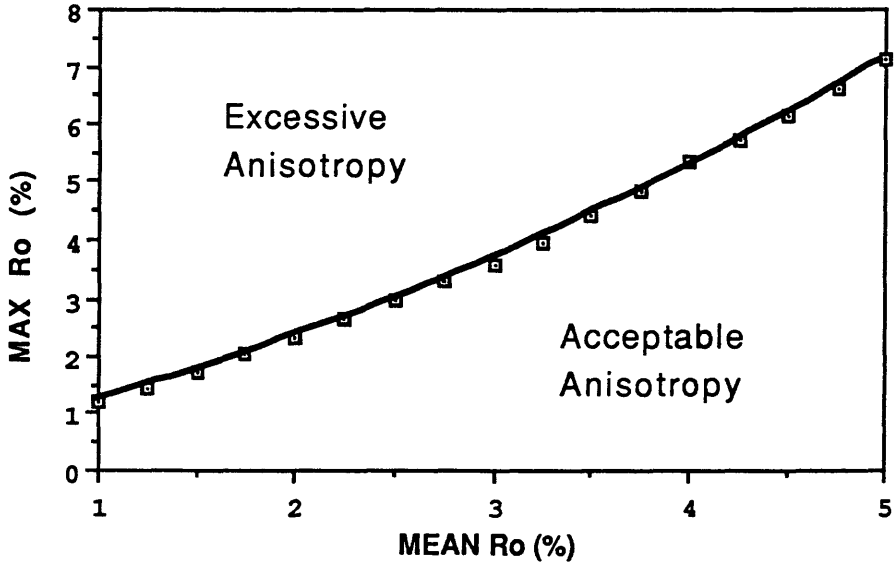

Figure 4. Plot of mean vitrinite reflectance (R_m) versus maximum vitrinite reflectance (R_{max}), showing the effects of increasing bireflectance with coal rank. These data (*from* Stach et al., 1982, Figure 19A) were used to help identify non-indigenous vitrinite particles and eliminate suspect data. For a given value of mean reflectance, individual data points should not exceed the expected "window" for R_{max}; values in excess of this threshold (i.e., in the field of excessive anisotropy) were omitted from final calculations of mean Ro.

the analyses of coal completed by Stach et al. (1982). Only when higher values fall outside of these limits for R_{max} [Figure 4] are data points eliminated from a second calculation of mean reflectance; this statistical filtering seldom involves more than a few (2-5) data points and has a minimal effect on values of mean reflectance (i.e., <0.1%R_m). Histograms showing the distribution of all reflectance values for each sample are shown in Appendix A.

In several cases, multiple samples were collected from within a few tens of meters of one another to test for local variations within the Kandik basin. Most of these comparisons fall within $\pm$0.3%R_m, but two stations show more significant differences between samples [Appendix B]. Because of these discrepancies (as well as the differences in statistical methods and other possible causes of interlaboratory scatter), mean values are reported herein to the nearest 0.1%R_m, even though analytical sensitivity extends to 0.01%R_o.

Paleotemperature

Several approaches have been proposed to convert values of mean reflectance to estimates of maximum paleotemperature. Some of these methods consider the effects of both peak temperature and effective heating time (Hood et al., 1975; Bostick et al., 1978; Waples, 1980), whereas others view R_m as an absolute indicator of peak paleotemperature for most geologic situations (Bostick, 1979; Price, 1983; Barker, 1983; Barker and Pawlewicz, 1986; Barker, written communication, 1987). This second viewpoint is based upon evidence indicating that reactions become stabilized after heating durations in excess of 1 million years (e.g., Barker, 1983). Moreover, stabilization of coal rank appears to occur sooner when the temperature is higher because of increases in the rate of the reactions (Kisch, 1987). Of the time-independent correlations, the Price (1983) curve yields the highest temperature values for a given R_m, whereas Barker (1987) yields the lowest. Differences between the respective temperature estimates increase progressively with metamorphic grade. Citing evidence from independent methods of geothermometry, it has been suggested that the Price (1983) correlation loses accuracy (temperatures are too high) above a rank of approximately 1.3%R_m (see Kisch, 1987). Consequently, we believe that the Barker (1987) equation [Table 2] produces the most accurate results over the range of metamorphic conditions documented in our study.

In the case of Kandik basin, assessments of effective heating time and accurate reconstructions of burial history are difficult to make because of large uncertainties regarding the absolute timing of depositional and tectonic events. Thus, large systematic errors could be introduced into analyses of time-dependent maturation trends, assuming those approaches are valid to begin with. On the other hand, if post-orogenic cover sequences truly are as old as Albian, and the uppermost strata within the Kandik River block (Kathul Graywacke) are as young as early Albian, then the heating event responsible for peak metamorphism of those strata must have been short lived (less than 10 m.y.). Given this relatively brief interval of time, the time-dependent and time-independent methods yield estimates of paleotemperature that are in fairly close agreement. To allow for appropriate comparison, we have calculated paleotemperatures using five different methods and three different effective heating times [Table 2]; all of the resulting values are shown in Table 3. The errors on these estimates are at least $\pm$30°C (see Underwood, 1989, for discussion of error analysis); because of this level of error, all data derived from the respective correlation equations have been rounded off to the nearest 10°C.

TABLE 2. CORRELATION EQUATIONS FOR CONVERSION FROM Rm (%) to MAXIMUM PALEOTEMPERATURE (°C)

Reference	Heating Time	Equation
Price (1983)	independent	$T\ (°C) = 131(ln\ Rm) + 187$
Barker & Pawlewicz (1986)	independent	$T(°C) = 128(ln\ Rm) + 154$
Barker (1987)	independent	$T(°C) = 104(ln\ Rm) + 148$
Bostick (1979)	independent	$T(°C) = 181 + 102(ln\ Rm) - 19\ [ln\ (Rm^2)] - 14\ [ln\ (Rm^3)]$
Bostick et al. (1978)	1 m.y.	$T(°C) = 192 + 85(ln\ Rm) - 13\ [ln\ (Rm^2)]$
Bostick et al. (1978)	10 m.y.	$T(°C) = 153 + 85(ln\ Rm) - 13\ [ln\ (Rm^2)]$
Bostick et al. (1978)	40 m.y.	$T(°C) = 132 + 85(ln\ Rm) - 13\ [ln\ (Rm^2)]$

TABLE 3. PALEOTEMPERATURE ESTIMATES (°C), KANDIK BASIN, ALASKA

		Paleotemperature Conversion Method						
Sample No.	R_m (%)	1	2	3	4	5	6	7
786-3-2c	0.6	120	90	100	130	150	110	90
786-3-2d	0.9	170	140	140	170	180	140	120
786-4-2c	0.7	140	110	110	140	160	120	100
786-7-3a	2.8	320	290	260	250	270	230	210
786-8-2a	3.5	350	310	280	250	280	240	220
786-8-2b	3.3	340	310	270	250	270	230	210
786-12-1d	3.7	360	320	280	250	280	240	220
786-13-1	2.1	280	250	220	240	250	210	190
786-14-1	3.3	340	310	270	250	270	230	210
786-14-3	3.5	350	320	280	250	280	240	220
786-14-4	4.2	370	340	300	250	290	250	230
786-22-1	0.9	170	140	140	170	180	140	120
786-23-1a	2.1	280	250	220	240	250	210	190
786-23-1b	1.8	260	230	210	230	240	200	180
786-23-2	1.7	260	220	200	230	230	190	170
786-23-3	2.2	290	260	230	240	250	210	190
786-25-8a	2.2	290	260	230	240	250	210	190
786-25-8b	1.8	260	230	210	230	240	200	180
786-25-10	1.6	250	210	190	220	230	190	170
786-26-1a	2.5	300	270	240	250	260	220	200
786-26-1b	2.9	330	290	260	250	270	230	210
786-27-1a	1.9	270	240	210	230	240	200	180
786-27-1b	1.6	250	220	200	220	230	190	170
786-27-2a	1.8	270	230	210	230	240	200	180
786-27-4a	2.7	320	280	250	250	260	220	200
786-27-4b	3.5	350	310	280	250	280	240	220
786-29-1	2.0	280	240	220	240	240	200	180
786-30-3	1.1	200	170	160	190	200	160	140
786-31-3b	1.8	260	230	210	230	240	200	180
786-31-3c	1.6	250	220	200	220	230	190	170
786-31-5	2.1	280	250	220	240	250	200	190
786-1-2	0.7	140	110	110	140	160	120	100
85jcr-13	1.7	260	220	200	230	230	190	170
85jcr-24	0.8	160	130	130	160	170	130	110
85jcr-25b	1.0	180	150	140	180	190	150	130

1.) Price (1983)
2.) Barker and Pawlewicz (1986)
3.) Barker, written communication (1987)
4.) Bostick (1979)
5.) Bostick et al. (1978); Teff = 1 my
6.) Bostick et al. (1978); Teff = 10 my
7.) Bostick et al. (1978); Teff = 40 my

Illite Crystallinity

Methods of sample preparation for quantification of illite crystallinity followed those described by Underwood and Strong (1986b). Briefly, shales and slates were powdered and size-segregated by centrifugation to isolate the <2μ size fraction. X-ray scans (using $CuK_{\alpha 2}$ radiation at a wavelength of 1.54059Å) were completed on oriented slides using a Scintag PADV microprocessor-controlled X-ray diffractometer. This fully automated instrument is interfaced with a Micromax 2000 microcomputer. Machine settings and processing parameters were as follows: voltage = 40 kV; amperage = 30 mA; chopper increment = 0.03°; receiver slit = 0.3 mm; noise threshold = 1.5; ESD multiplier = 4.0; points for smoothing = 3; scanning rate = 1°/min . Sample holders were spun during the analyses. Specimens were saturated with ethylene glycol to shift the 14Å expandable-clay peak to 17Å; this treatment reduces the potential interference of mixed-layer (smectite-illite) phases with the 10Å illite peak.

Digital data obtained from fast-continuous X-ray scans (run from 3° to 11°2θ) were processed through a background correction and a deconvolution routine, and the peak widths at one-half peak height were calculated automatically [Figure 5]. This peak measurement follows the criteria originally established by Kubler (1968); peak widths, otherwise known as crystallinity index (**CI**), are expressed in terms of Δ°2θ, rather than mm; this procedure minimizes the effects of variations in scanning and recording parameters (see for example, Kisch, 1980; Duba and Williams-Jones, 1983). Peak widths become more narrow (smaller CI) with increasing levels of diagenesis-metamorphism due to the increasing size of authigenic illite crystals.

Two tests for internal reproducibility using the Scintag diffractometer (each involving 11 splits of a single sample) yielded standard deviations of only 0.009Δ°2θ and 0.015Δ°2θ. Ideally, the values of illite crystallinity are attributed to indigenous burial temperatures, but crystallinity can be influenced or distorted by variations in the original clay chemistry, the presence of mixed-layer clay phases, detrital clay particles mixed with authigenic illite, pore-fluid chemistry, structural deformation, short-period magmatic heating, and weathering (Gaudette et al., 1966; Dunoyer de Segonzac, 1970; Perry and Hower, 1970; Reynolds and Hower, 1970; Hower et al., 1976; Kisch, 1987; Dorsey et al., 1988). Moreover, because the crystallinity of illite has never been calibrated systematically against temperature (using, for example, direct borehole measurements), the method should be regarded only as a semi-quantitative means of assessing relative diagenetic-metamorphic grade. All results reported herein are rounded off to the nearest 0.01Δ°2θ [Appendix B], even though analytical sensitivity extends to 0.001Δ°2θ.

Organic Geochemistry

Programmed pyrolysis (Rock-Eval) generates several types of data that can be used to evaluate petroleum source-bed potential. A flame ionization detector senses any organic compounds generated during pyrolysis. All analyses in this study were completed on powdered bulk samples rather than kerogen residues. The first peak generated during pyrolysis (**S1**) represents hydrocarbons that are thermally distilled from the rock. The second peak (**S2**) signifies hydrocarbons generated by pyrolitic degradation of the kerogen in the rock. The third peak (**S3**) records carbon dioxide generated during temperature programming up to 390°C. In addition, analytical output includes the total quantity of organic carbon (**TOC**), expressed in units of wt-% organic carbon.

The hydrogen index (**HI**) corresponds to the quantity of hydrocarbons from S2 relative to TOC [(*mg* HC/*g* TOC) x 100], and the oxygen index (**OI**) corresponds to the quantity of carbon dioxide from S3 relative to TOC [(*mg* CO_2/*g* TOC) x 100]. Plots of HI versus OI (modified van Krevelen

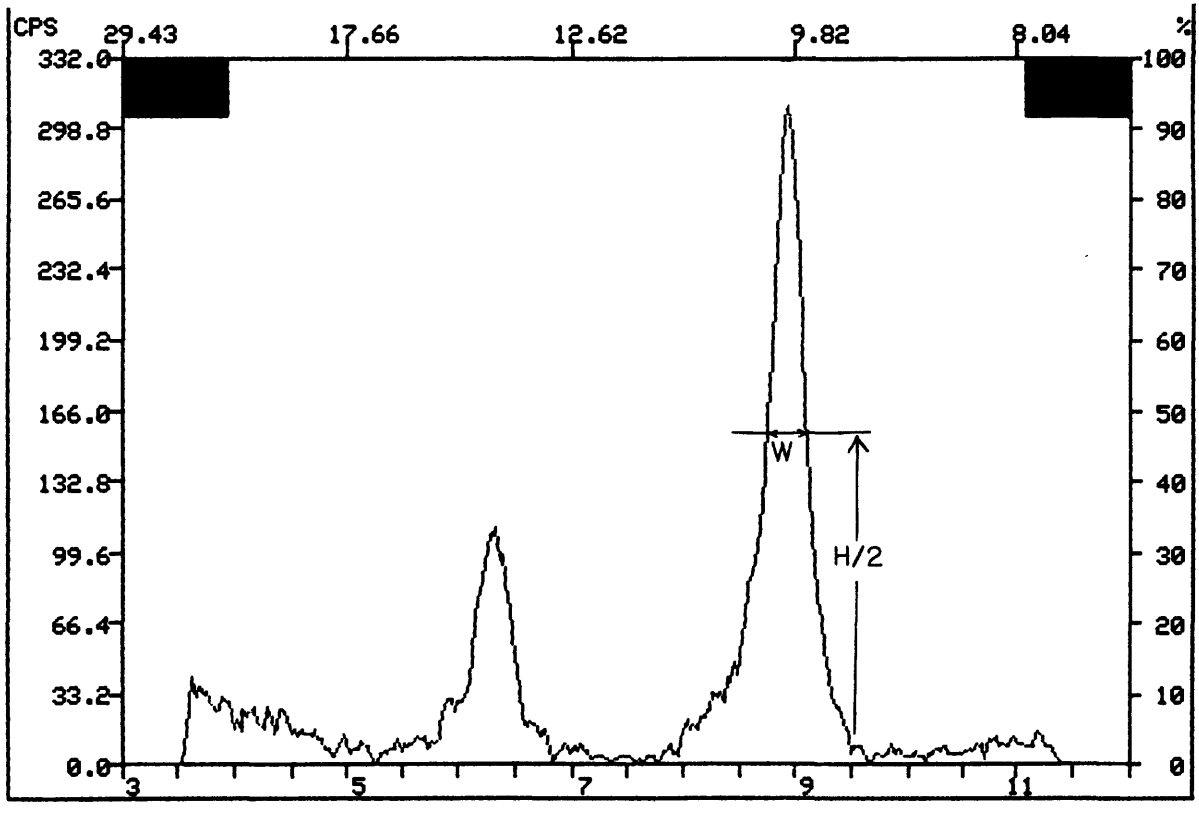

Figure 5. Computer graphics output of a typical X-ray diffractogram showing the 10Å illite peak and the method of measuring peak width at one-half peak height (crystallinity index of Kubler, 1968). These measurements were made automatically by a computer program following a base line correction and deconvolution of the 10Å peak. Data are expressed in units of $\Delta°2\theta$. Lower horizontal scale is in $°2\theta$; upper horizontal scale is in Å. Vertical scales are in cycles per second and %cps. The peak at approximately 14Å is due to chlorite.

diagram) are used to classify types of organic matter; Type I (hydrogen-rich) is very oil prone, Type II is oil prone, Type III is gas prone, and Type IV (hydrogen depleted) is inert kerogen. The temperature at which the maximum amount of S2 hydrocarbons is generated is termed **TMAX**, and levels of thermal maturation can be estimated from these values. TMAX values greater than 580° signify overmature conditions; actual values for samples at this level of thermal maturity were not recorded by the laboratory technician (see Appendix C). The production index (**PI**) is defined as the ratio $S_1 \div (S_1+S_2)$, and this value also serves as a measure of thermal maturity. Additional information concerning the applications and limitations of Rock-Eval data can be found in Espitalie et al. (1977), Clementz et al. (1979), Katz (1983), and Peters (1986).

RESULTS

Tectonostratigraphic Framework

All sampling stations are shown on Figure 6. The resulting data sets have been subdivided into two distinct groups based upon the position of sampling stations with respect to the Glenn Creek fault zone. Thirty-five samples were analyzed from the Kandik River block (northwest side); 34 of these shales and slates are from either the Glenn Shale or the Kandik Group (Biederman Argillite + Kathul Graywacke), and one sample (85jcr-11) was obtained from Devonian-Mississippian strata (Ford Lake Shale) exposed within the core of the Step Mountain anticline [Figure 6]. One sample (786-7-3) was collected near the main fault trace of the Glenn Creek system. Samples from southeast of the Glenn Creek fault (Nation River block) are restricted to Proterozoic and Paleozoic rock units. Most of these specimens were collected from the Nation River Formation (Devonian); the oldest rocks analyzed for vitrinite reflectance come from the Road River Formation (Ordovician-Devonian).

Vitrinite Reflectance

Results from analyses of vitrinite reflectance are tabulated in Appendix B. Overall, the level of organic metamorphism varies considerably across the Kandik basin region [Figure 7]. The standard deviations with respect to values of mean reflectance increase uniformly with metamorphic grade because of the effects of bireflectance [Figure 3]. As discussed previously, polymodal histogram trends and unusually large standard deviations (>0.6%R_m) are problematic because they could be caused by vitrinite recycling or by a maceral group (other than vitrinite) that remains unrecognized during optical examination of small dispersed particles. Consequently, samples with abnormal standard deviations are probably less reliable for assessing indigenous thermal maturity.

With one exception, values of mean vitrinite reflectance from the Nation River block range from 0.6% to 1.2%; a single anomaly of 2.1% is evident at site 786-29-1, which is located approximately 8 km from the Glenn Creek fault [Figure 7]. Discounting that anomaly, the remaining values all fall within the window of peak oil generation [Figure 8]. According to the correlation of Barker (written communication, 1987), these R_m values correspond to paleotemperatures of 100°C to 220°C; temperatures based upon the other conversion methods are shown in Table 3.

Mesozoic samples from the Kandik River block (including one sample from the fault zone itself) display significantly higher levels of thermal maturity than older strata assigned to the Nation River block [Figure 7]. R_m values range from 1.6% to 4.2% [Figure 9]. All of these data fall below the floor of oil generation [Figure 9], and most samples are overmature with respect to wet gas (the wet-gas floor = 2.0%R_m). Using the Barker (1987) equation, the corresponding

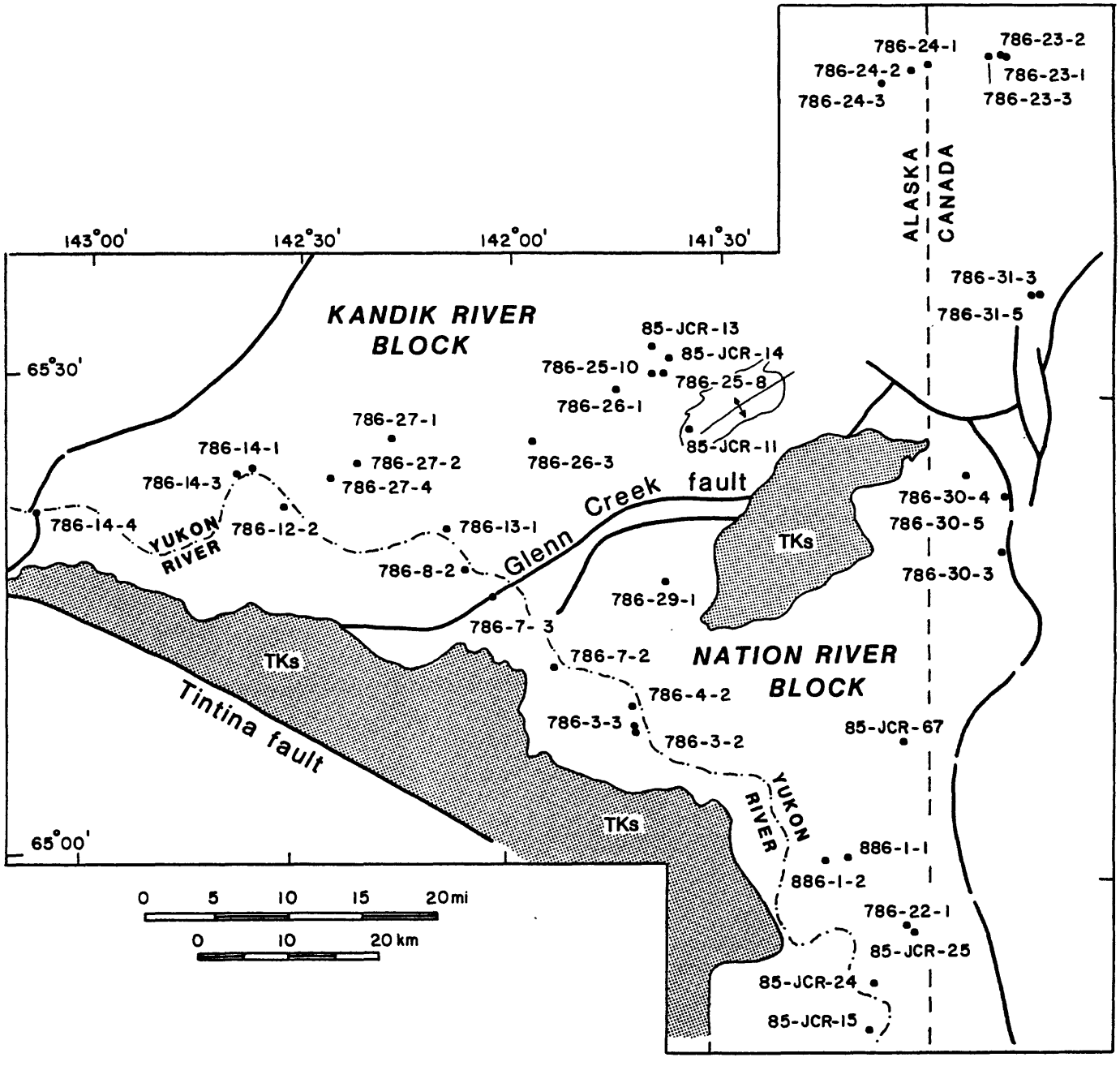

Figure 6. Map of the Kandik basin study area showing the locations of all sampling stations. Stippled pattern highlights undifferentiated non-marine cover sequences of Cretaceous and Tertiary age (TKs).

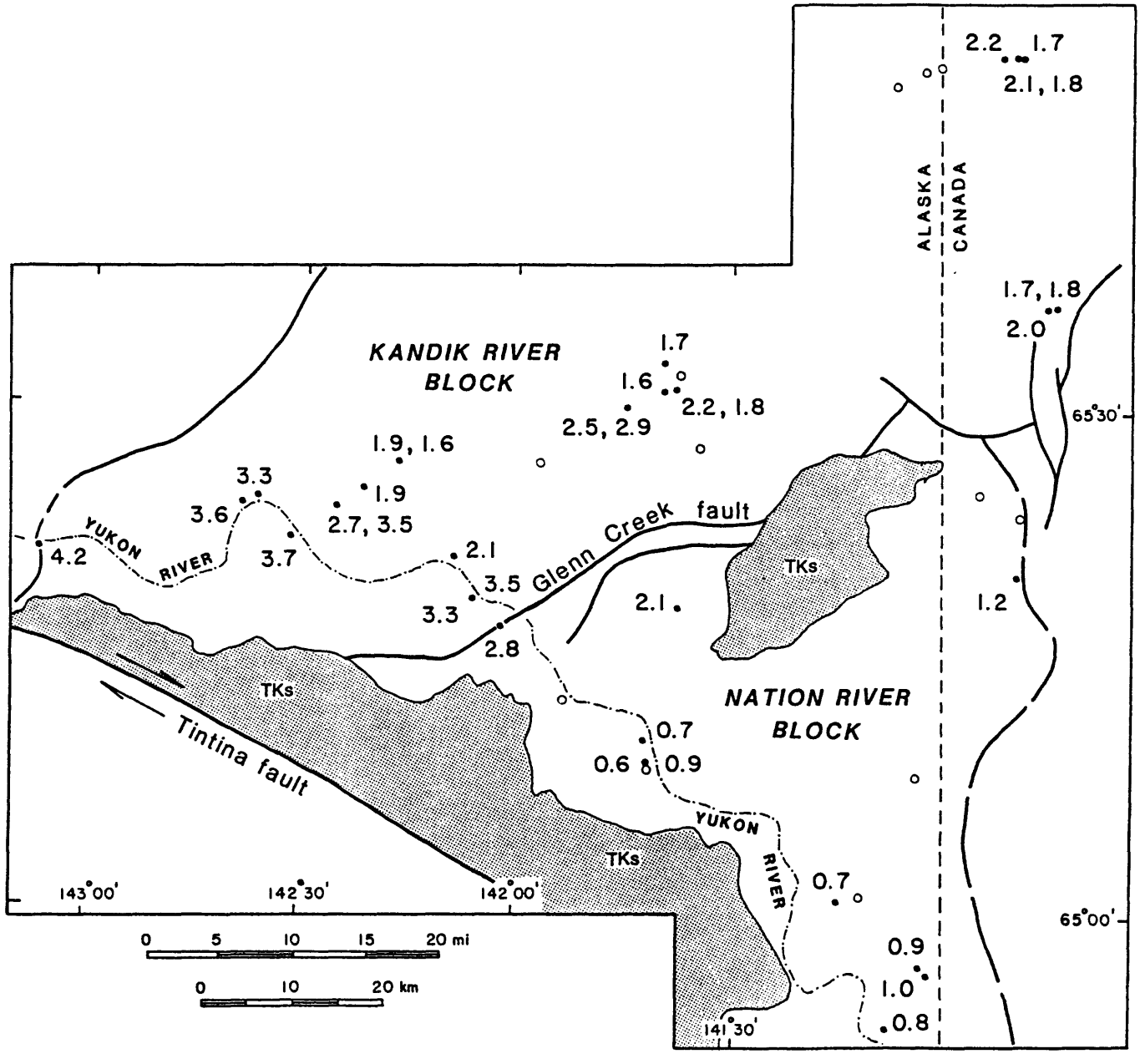

Figure 7. Map of the Kandik basin study area showing values of mean vitrinite reflectance (Rm%). Open circles indicate samples with insufficient vitrinite for proper analysis. Stippled pattern highlights undifferentiated non-marine cover sequences of Cretaceous and Tertiary age.

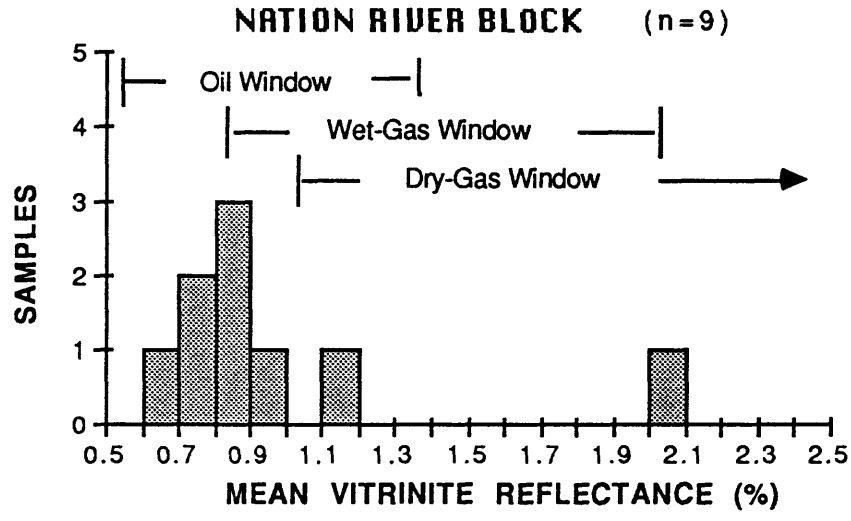

Figure 8. Histogram showing values of mean vitrinite reflectance (R_m%) for strata of the Nation River block. Corresponding windows for oil, wet-gas, and dry-gas generation are from Dow (1977).

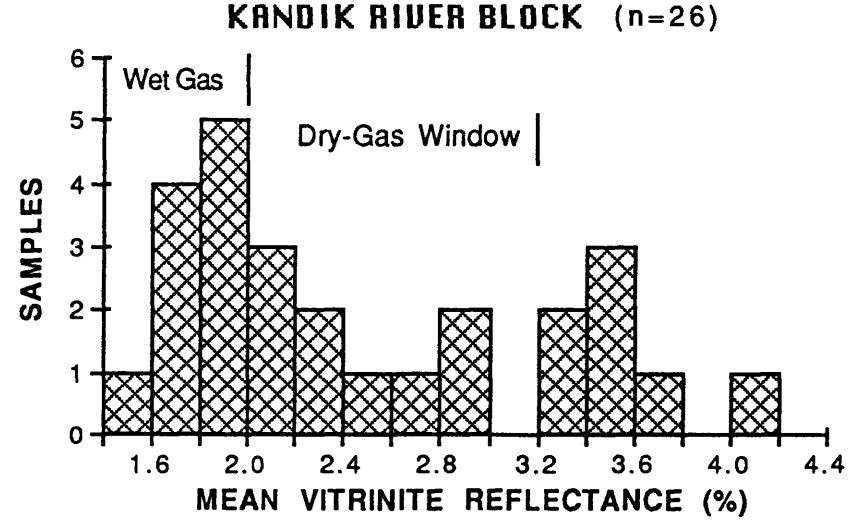

Figure 9. Histogram showing values of mean vitrinite reflectance (R_m%) for strata of the Kandik River block. Corresponding windows for petroleum generation are from Dow (1977).

paleotemperatures range from 190°C to 300°C [Table 3].

There is an obvious inversion between stratigraphic position and levels of thermal maturity; Cretaceous strata within the Kandik River block show the highest levels of organic metamorphism, whereas Devonian rocks in the Nation River block show the lowest amount of thermal alteration. This inverse relation was first described in the field by Churkin and Brabb (1969). A normal paleothermal gradient may be intact within the Cretaceous section, as R_m values for the Biederman Argillite are consistently higher than those of the overlying Kathul Graywacke (mean R_m = 1.8%).

Illite Crystallinity

The primary purpose of analyzing illite crystallinity was to provide independent quantification of diagenetic-metamorphic conditions as a check on the reliability of vitrinite data. Moreover, estimates of thermal maturity could be made for Proterozoic and Cambrian strata that contain no vitrinite. We stress, however, that CI and R_m cannot be correlated directly in all cases because each is influenced to some degree by different sets of physical and chemical factors (e.g., Frey et al., 1980; Kisch, 1987).

The statistical correlation between R_m and CI in Kandik basin is shown in Figure 10; the correlation coefficient ($r = 0.67$) is statistically significant at a confidence level of 0.005, and this value represents a better statistical fit than comparable results from other studies (e.g., Guthrie et al., 1986). Moreover, Figure 11 shows that the same general spatial trends are evident in CI data; in other words, illite displays a higher degree of crystallinity (lower CI) in the Kandik River block than in the Nation River block.

Samples from the Nation River block range from CI = 0.33 to CI = 0.67 [Figure 12], and the mean value for the entire block is 0.52Δ°2θ. It is important to note, however, that the two lowest CI values (highest metamorphic grade) were obtained from Proterozoic basement strata [Figure 12]. The mean value for the Paleozoic specimens is 0.55Δ°2θ. Based upon the studies of Kisch (1980), this level of crystallinity clearly falls within the zone of diagenesis.

In comparison, samples from the Kandik River block range from CI = 0.28 to CI = 0.83 [Figure 13], and the mean value is 0.46Δ°2θ. One Paleozoic sample from the northwest fault block (85jcr-11) was too lean for Ro analysis, but this mudrock also displays a high degree of crystallinity (CI = 0.37). The boundary between diagenesis and anchimetamorphism (beginning of incipient metamorphism) is placed by most workers at 0.37-0.42Δ°2θ, and the upper limit of the anchimetamorphic zone (transition into epimetamorphism) occurs at approximately 0.21-0.24Δ°2θ (see Kisch, 1987). Thus, nearly half of the samples from the Kandik River block fall within the anchizone [Figure 13]. These data effectively confirm the results from analyses of organic metamorphism, as the boundary between diagenesis and anchimetamorphism occurs at an R_m value of 2.3% to 3.1%; the upper limit of anchimetamorphism occurs at an R_m value of approximately 5.0% (Kisch, 1987).

Geochemical Data

Rock-Eval pyrolysis was completed to assess source-bed potential, to quantify kerogen type, and to provide another independent check on levels of thermal maturity. No significant differences in kerogen type or TOC were recorded as a function of stratal age or structural position [Appendix C]. TOC values range from 0.15 wt-% to 5.26 wt-% [Figure 14], and the average carbon content for 45 samples is 0.98 wt-%. Most acknowledged source beds for hydrocarbons contain between 0.8 and 2.0 wt-% TOC, so these strata definitely represent viable sources for petroleum [Figure

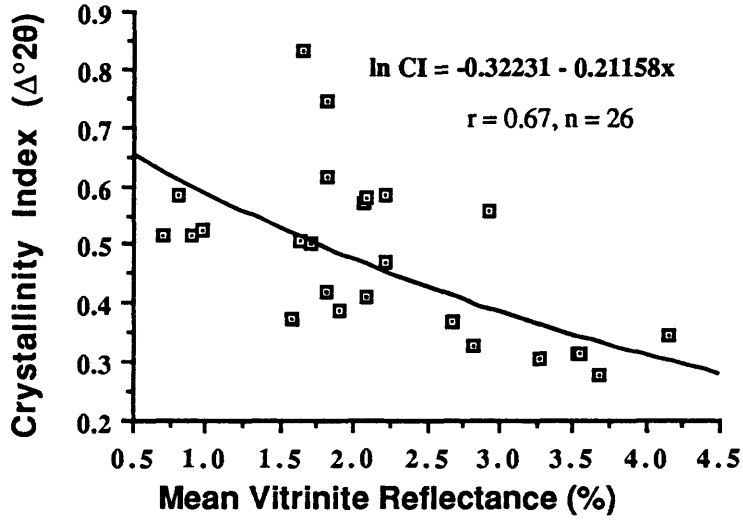

Figure 10. Regression plot of mean vitrinite reflectance versus illite crystallinity index for samples obtained from the Kandik basin region. Correlation coefficient (r = 0.67) means that this exponential curve fit is statistically significant at the 0.005 confidence level.

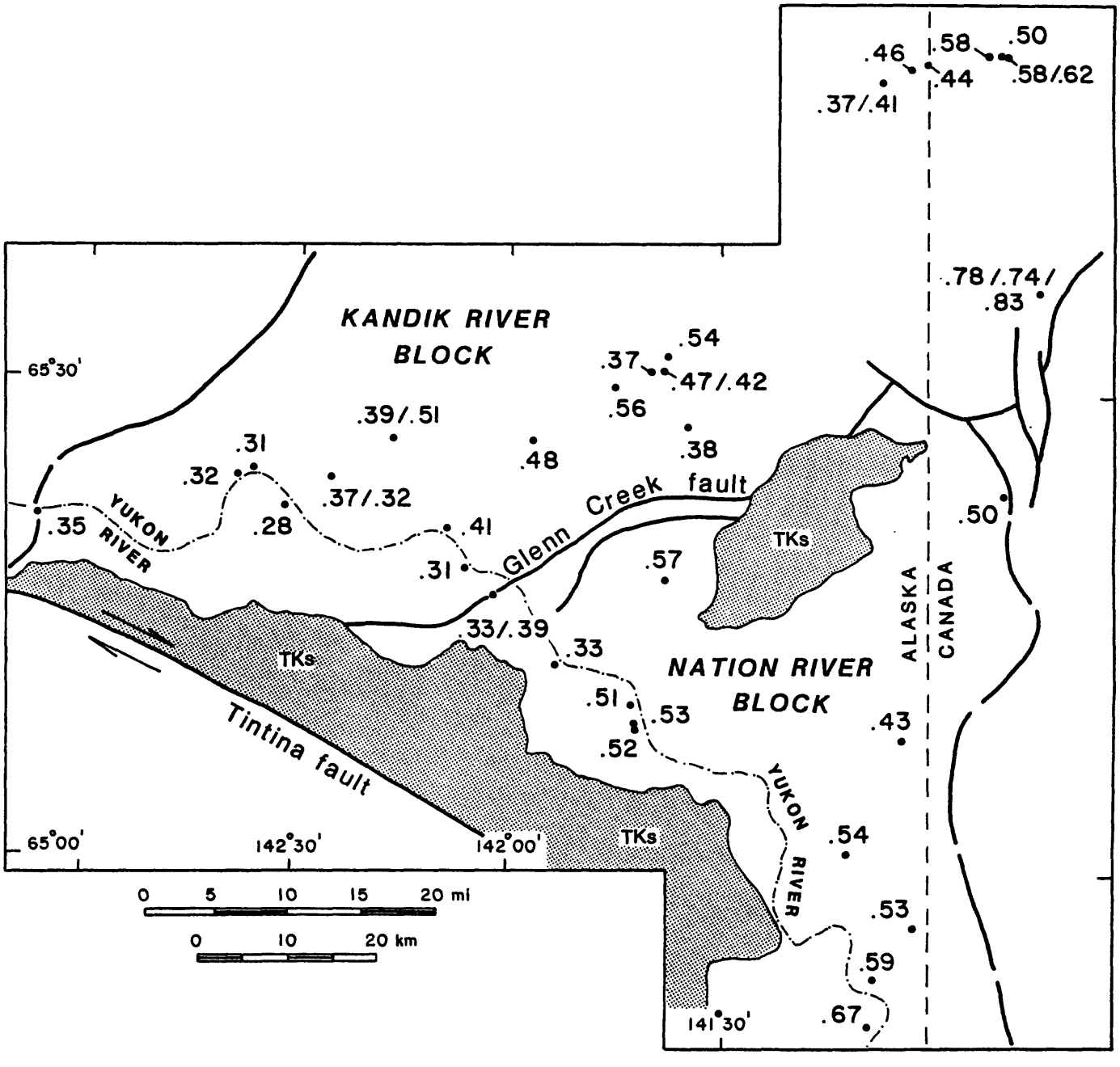

Figure 11. Map of the Kandik basin study area showing values of illite crystallinity index (CI) in units of $\Delta°2\theta$. Stippled pattern highlights undifferentiated non-marine cover sequences of Cretaceous and Tertiary age.

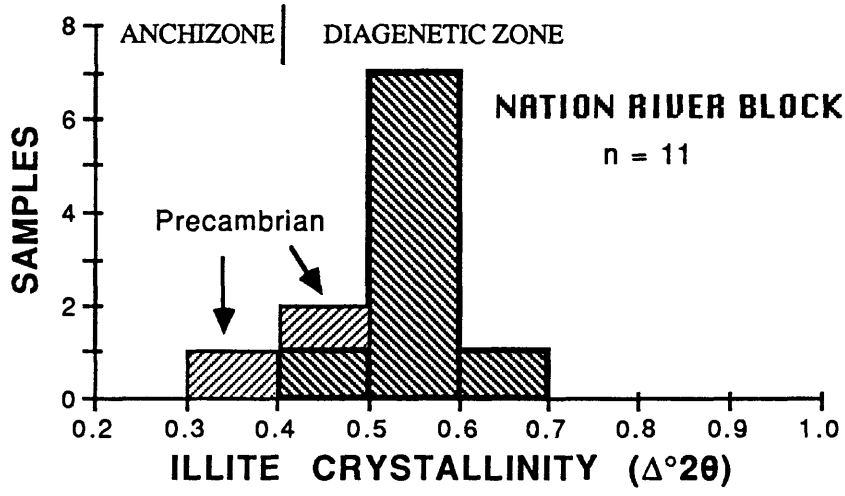

Figure 12. Histogram showing values of illite crystallinity index (Δ°2θ) for strata of the Nation River block. Corresponding limits for zones of diagenesis and anchimetamorphism are from Kisch (1980). Note that the two highest values were obtained from Precambrian basement sequences of the Tindir Group.

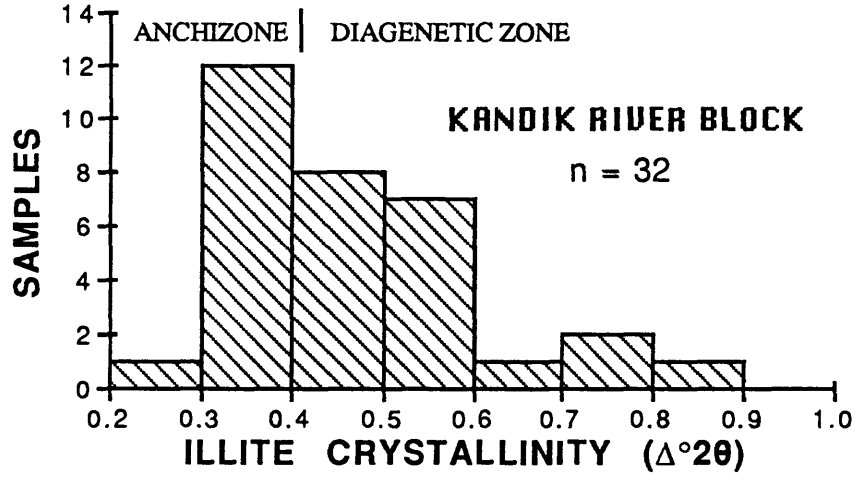

Figure 13. Histogram showing values of illite crystallinity index (Δ°2θ) for strata of the Kandik River block. Corresponding limits for zones of diagenesis and anchimetamorphism are from Kisch (1980).

14]. Stratigraphic intervals of oil shale within the Glenn Shale also attest to the potential for hydrocarbon generation. There is no meaningful relationship between TOC content and mean vitrinite reflectance [Figure 15].

Most of the HI and OI data fall within the established boundaries of Type III (gas prone) or Type IV (inert) kerogen [Figure 16]. Only three samples yielded HI values greater than 150, and these results show only a slight trend toward Type II kerogen. Thus, there is little likelihood for generation of significant amounts of oil. Many of the low values of both HI and OI are probably due to overmature conditions. Nevertheless, the evidence from sub-mature samples (i.e., R_m<1.3%) also shows an absence of Type II and Type I kerogens. This result is important because R_m values can be suppressed by high concentrations of hydrogen-rich organic matter (see Price and Barker, 1985, for a discussion of this problem).

Production indices are no greater than 0.25, and many PI values are equal to 0.00 [Appendix C]. This is because most samples yielded very small S_1 peaks during low-temperature thermal distillation [Appendix C]. Measurable T_{MAX} values range from 429°C to 579°C; many of the test results were not recorded, however, because they exceeded 580°C. Previous workers have suggested that values above 470°C indicate conditions that are overmature with respect to the oil window (e.g., Peters, 1986), and this level of maturity is approximately equal to R_m = 1.4%. The correlation, however, between R_m and T_{MAX} data from Kandik basin is not statistically significant at the 0.05 level of confidence [Figure 16]. The reasons for this poor correlation are not entirely clear, but T_{MAX} can be adversely affected by variations in kerogen type, TOC content, and mineral matrix (Espitalie et al., 1980; Peters, 1986). More importantly, published comparisons between T_{MAX} and R_m typically omit strata that are postmature (e.g., Peters, 1986); the correlation is probably invalid under anchimetamorphic conditions due to progressive depletion of hydrocarbons. Consequently, we do not place much faith in the T_{MAX} values as reliable indicators of thermal maturity for higher grade rocks from Kandik basin.

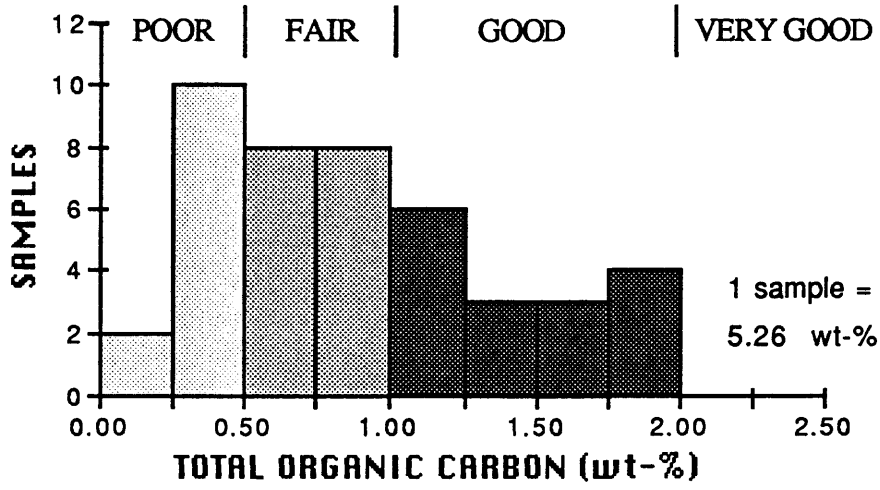

Figure 14. Histogram showing values of total organic carbon (wt-%) for samples from the Kandik basin region. Designations for quality of petroleum source beds (poor, good, fair, very good) are from Peters (1986).

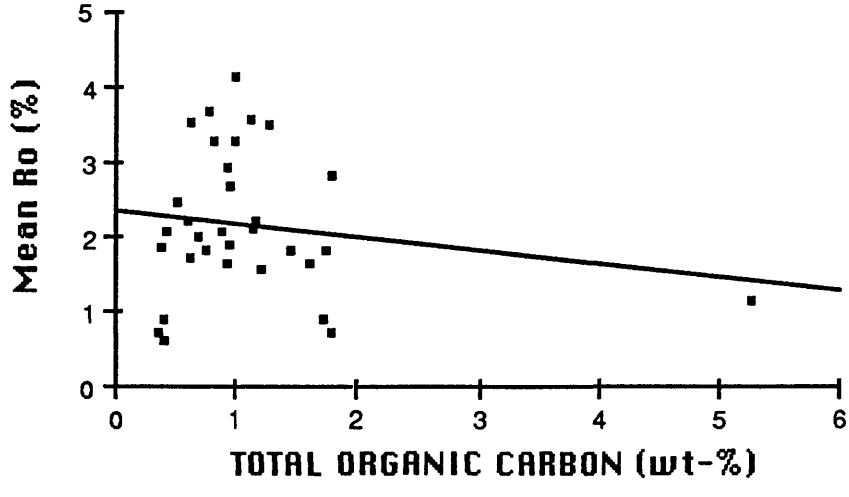

Figure 15. Linear regression plot of total organic carbon (wt-%) versus mean vitrinite reflectance (Rm%) for samples from the Kandik basin region. This correlation (r = 0.2) is not statistically significant at a confidence level of 0.05.

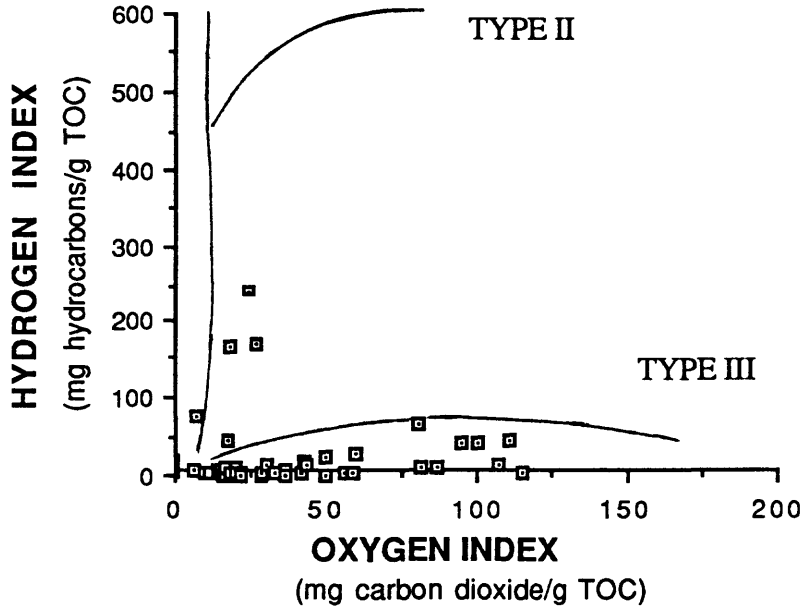

Figure 16. Modified van Krevelen diagram showing values of hydrogen index (HI) and oxygen index (OI) as determined by Rock-Eval pyrolysis. All samples are from the Kandik basin region, and raw data are tabulated in Appendix C. According to Peters (1986), these data correspond to Type III (gas-prone) and Type IV (inert) kerogens.

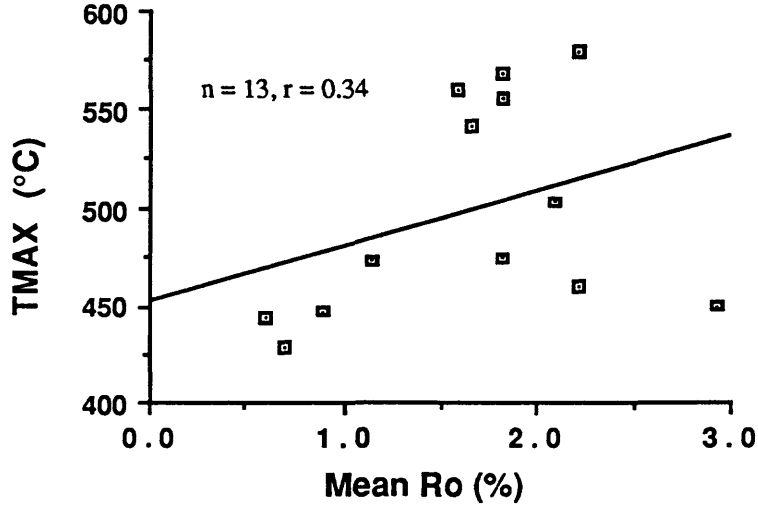

Figure 17. Linear regression plot of mean vitrinite reflectance (R_m%) versus TMAX (°C). All samples are from the Kandik basin region of Alaska. TMAX data were obtained from Rock-Eval pyrolysis and represent the temperatures at which the maximum amount of S2 hydrocarbons (mg HC/g rock) are generated. The correlation ($r = 0.34$) is not statistically significant even at a confidence level of 0.05.

DISCUSSION

Indicators of both organic and inorganic metamorphic grade define a stark contrast between the dominantly Cretaceous samples northwest of the Glenn Creek fault and the dominantly Devonian samples from southeast of the fault. The average paleotemperature contrast between the respective fault blocks is 100°C to 130°C, depending upon which Rm-Temp conversion is used [Figure 18]. The maximum contrast in paleotemperature is 200°C to 250°C [Figure 18]. Oddly enough, the younger samples display the highest levels of metamorphism, and this unexpected relationship must be accounted for as part of any interpretation of regional tectonic and thermal evolution.

The timing of peak heating within the Nation River block remains uncertain, but if one assumes a surface temperature of 10°C (or less) and a linear geothermal gradient of approximately 30°C/km, then the maximum burial temperature (220°C, following Barker, 1987) requires a burial depth of approximately 7 km. The average paleotemperature for the Nation River block (145°C) requires only 4.5 km of burial, and this value is approximately equal to the cumulative thickness of the Mesozoic section within the Kandik River block (taken from the stratigraphic estimates of Brabb and Churkin, 1969). Erosional events during Pennsylvanian, Permian, and Mesozoic (?) time removed unknown amounts of overburden. The Cretaceous-Tertiary nonmarine overlap sequence could be responsible for burial, as well. Thus, the overburden required for thermal maturation of the Nation River block is relatively easy to account for.

On the other hand, metamorphism of the Kandik River block, which must have occurred during Albian time, remains an enigma. Again, using an assumed geothermal gradient of 30°C/km, the average paleotemperature of 240°C means that most strata within this fault block require burial depths of about 8 km, and the maximum depth (at $R_m = 4.2\%$ and 300°C) may have approached 10 km. Burial to these depths is difficult to imagine, but at least four possible scenarios should be considered: (1) depositional and/or structural burial of the Kandik River sequence beneath a cryptic cover terrane, followed by uplift and erosion either prior to or during movement along the Glenn Creek fault system, (2) structural burial of the Kandik River block as a consequence of northwest-directed overthrusting along the Glenn Creek fault, (3) post-orogenic burial beneath the Upper Cretaceous to Tertiary sequences that unconformably cover both fault blocks, or (4) exhumation of higher grade rocks by normal (detachment) faulting.

Sedimentary burial of the Kandik River block beneath post-orogenic cover sequences following early Albian time is not a viable solution because the thickness of the overlap assemblage (roughly 1 km maximum) is nowhere near the overburden required for the documented levels of metamorphism, unless the geothermal gradient had been *exceptionally* high at the time of metamorphism. More importantly, this explanation does not account for the disparity in metamorphic grade across the Glenn Creek fault zone.

The hypothesis of a southeast-dipping, older-over-younger, normal fault [Figure 19a] cannot account for the dramatic inversion in metamorphic grade between Mesozoic formations of the northwest block and Paleozoic units to the southeast. In essence, this normal-fault mechanism fails to resolve how older rocks were initially emplaced over younger rocks; in addition, it fails to provide either a mechanism responsible for deep burial and Cretaceous metamorphism of the "horst" or a mechanism for isolating the "hanging wall" from the effects of that metamorphic event. A northwest-dipping, younger-over-older detachment contradicts the sense-of-motion requirement for uplift and erosion of the Kandik River block.

Structural burial of the Kandik River block due to overthrusting is a possibility that requires further consideration [Figure 19b]; this interpretation is consistent with an older-over-younger,

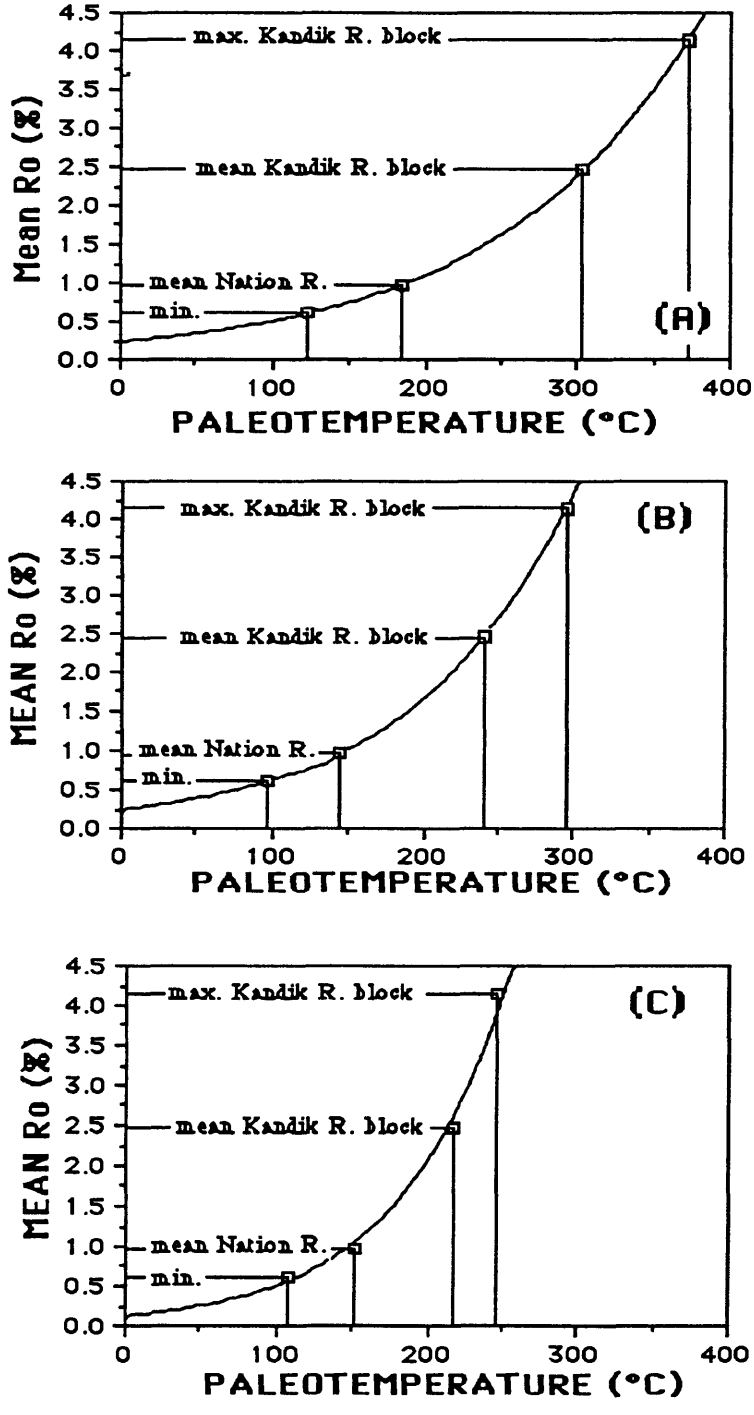

Figure 18. Average and maximum contrasts in paleotemperature across the Glenn Creek fault using three methods for converting R_m to °C. **Figure 18A** follows the time-independent correlation of Price (1983). **Figure 18B** follows the time-independent correlation of Barker (written communication, 1987). **Figure 18C** follows the time-dependent method of Bostick et al. (1978) and assumes an effective heating time of 10 m.y. Equations for the three respective correlation lines are shown in Table 2.

southeast-dipping thrust (as suggested by Howell and Wiley, 1987). Under these circumstances the paleotemperatures attained and within the basal portion of the hanging wall should be close to those of the uppermost footwall because of conductive heat transfer across the fault plane (e.g., Brewer, 1981; Angevine and Turcotte, 1983; Furlong and Edman, 1984). Higher degrees of maturation would occur at deeper levels the footwall because of the cumulative thickness of the overthrust sheet and the internal stratigraphy of the footwall. The available data, however, are insufficient to show whether consistent thermal-maturity gradients exist as a function of horizontal distance from the fault zone or structural position beneath or above the fault. In addition, this mechanism fails to explain how high-grade rocks within the inferred footwall were elevated to the surface. Perhaps the southeast-dipping thrust post-dated peak metamorphism and cooling of both fault blocks, but then the fault would simply truncate inherited metamorphic trends rather than providing the heat necessary for metamorphism.

As a final scenario for consideration, a pre-thrust (Albian?) metamorphic event could be combined with displacement along a northwest-dipping fault [Figure 19c]. This fault geometry would require a younger-over-older thrust relationship; the model does not explain how or where the metamorphism occurred, but it does provide a viable mechanism for the simultaneous uplift and erosion of a thick Cretaceous overburden sequence. Sticking with the assumptions outlined previously (geothermal gradient of 30°C/km, etc.), the maximum paleotemperature contrast across the fault (200-250°C) requires 6-8 km of total differential uplift. This total vertical displacement may have been distributed among several coeval faults within the Glenn Creek system, and the amount of absolute uplift can be reduced by choosing a higher geothermal gradient during Cretaceous time. Nevertheless, large amounts of overthrusting would account for the required uplift of the Kandik River block, and thrust sheets northwest of the Kandik River block could have provided the overburden required for burial. We prefer this model because it provides mechanisms for both rapid burial and subsequent uplift.

Accurate dating of the post-orogenic cover sequences remains a pivotal problem in the reconstruction of regional thermal and tectonic history. The existing stratigraphic framework identifies probable Albian strata (Kathul Graywacke) within the Kandik River block; it has also been suggested that the nonmarine overlap sequences are as old as Albian. If this information is correct, then the hiatus associated with the Albian unconformity appears to be no lengthier than 10 m.y.; therefore, the Kandik River block must have been uplifted and eroded quite rapidly. This need for rapid Albian denudation is easiest to accommodate along a system of northwest-dipping thrusts. Furthermore, by maintaining a rough balance between rates of uplift and rates of erosion, the structural overburden emplaced above the Nation River block would remain relatively thin. Under these circumstances, the elevated rock temperatures within the hanging wall would dissipate rapidly. Paleotemperature evidence would be preserved within the hanging wall because there are no retrograde effects with organic metamorphism. By maintaining a thin overthrust sheet, substantial amounts of heat would not be conducted across the fault plane into the footwall, and the inversion between metamorphic grade and stratal age would remain intact.

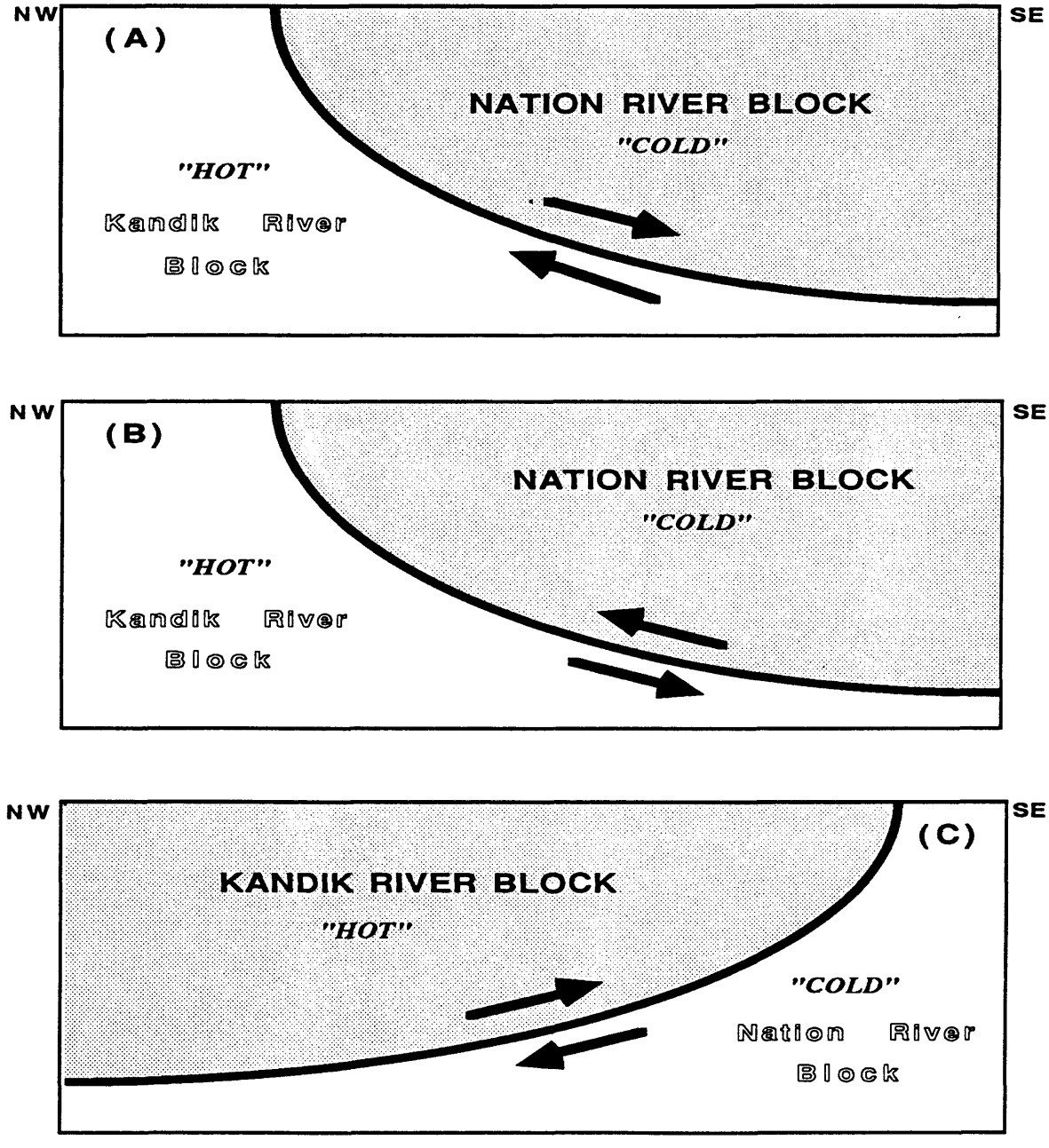

Figure 19. Models of thermal evolution for the Nation River block and the Kandik River block, Glenn Creek fault zone, Alaska. **Figure 19A** illustrates the possibility of a SE-dipping normal fault that exposes a more-mature horst block during regional uplift and crustal extension. See text for discussion of these interpretations. **Figure 19B** shows a SE-dipping, older-over-younger and "colder-over-warmer" thrust geometry, which is consistent with the interpretation of Howell and Wiley (1987) and the down-to-the-north designation shown by Brabb and Churkin (1969). **Figure 19C** depicts a NW-dipping, younger-over-older and "hotter-over-colder" thrust relationship; this model is consistent with the interpretation of Dover (1985) and Dover and Miyaoka (1988).

CONCLUSIONS

The stratal sections on either side of the Glenn Creek fault system display gross similarities in lithology and biostratigraphy, but both organic and inorganic indicators of metamorphism demonstrate that the thermal and burial histories of the fault blocks were dramatically different. In essence, paleothermal data prove that an allochthonous relationship exists between the Nation River block and the Kandik River block. Contrasts in paleotemperature between the fault blocks average approximately 100°C, and maximum variations are as high as 200-250°C. Paleozoic strata to the southeast of the fault zone were never exposed to unusually high geothermal gradients or subjected to more than a few km of burial, whereas Cretaceous rocks northwest of the fault zone were metamorphosed under lower greenschist facies conditions. The overburden, heat source, and tectonic setting responsible for peak metamorphism of the Cretaceous rocks all remain unaccounted for and, therefore, topics for additional investigations. The cryptic overburden section probably totaled 7-10 km in thickness, and burial evidently took place prior to fault dislocation, in a region located well outside the confines of the present study area. Thus, we conclude that impressive amounts of rapid uplift and horizontal slip must have occurred along the Glenn Creek fault system. These kinematic requirements are best accommodated through overthrusting along a northwest-dipping fault, and this tectonic event apparently occurred during middle to late Albian time. Additional work is required, however, to document gradients in thermal maturity with respect to distance from the fault zone.

In terms of potential for hydrocarbon generation, Devonian strata now at the surface of the inferred footwall (Nation River block) reached levels of thermal maturity coincident with the window of peak oil generation. Conversely, virtually all of the strata within the Kandik River block are presently overmature with respect to the oil window; many strata, however, remain above the floors of wet-gas and/or dry-gas generation. Most samples contain Type III (gas-prone) or Type IV (inert) kerogen. The Devonian and Cretaceous shales and slates remain relatively enriched in total organic carbon (1.0-5.0 wt-%) and, thus, could serve as productive source rocks.

REFERENCES CITED

Angevine, C.L., and Turcotte, D.L., 1983, Oil generation in overthrust belts: *AAPG Bulletin*, v. 67, p. 235-241.

Barker, C.E., 1983, Influence of time on metamorphism of sedimentary organic matter in liquid dominated geothermal systems, western North America: *Geology*, v. 11, p. 384-388.

Barker, C.E., and Pawlewicz, M.H., 1986, The correlation of vitrinite reflectance with maximum paleotemperature in humic organic matter, in G. Buntebarth and L. Stegena, eds., *Paleogeothermics*: New York, Springer-Verlag, p. 79-93.

Bostick, N.H., 1979, Microscopic measurement of the level of catagenesis of solid organic matter in sedimentary rocks to aid exploration for petroleum and to determine former burial temperatures - A review, in P.A. Scholle and P.R. Schluger, eds., *Aspects of diagenesis*: SEPM Spec. Publ. 26, p. 17-43.

Bostick, N.H., Cashman, S., McCollough, T.H., and Wadell, C.T., 1978, Gradients of vitrinite reflectance and present temperature in the Los Angeles and Ventura basins, California, in D. Oltz, ed., *Symposium in geochemistry: Low temperature metamorphism of kerogen and clay minerals*: SEPM Pacific Section, p. 65-96.

Brabb, E.E., 1969, Six new Paleozoic and Mesozoic formations in east-central Alaska: *USGS Bulletin*, v. 1274-I, p. 1-26.

Brabb, E.E., and Churkin, M., Jr., 1969, Geologic map of the Charley River Quadrangle, east-central Alaska: *USGS Misc. Geol. Invest. Map*, I-973, scale 1:250,000.

Brewer, J., 1981, Thermal effects of thrust faulting: *Earth Planet. Sci. Letters*, v. 56, p. 309-328.

Clementz, D.M., Demaison, G.J., and Daly, A.R., 1979, Well site geochemistry by programmed pyrolysis: *Proc. of the 11th Annual Offshore Tech. Conf.*, v. 1, p. 465-470.

Churkin, M., and Brabb, E.E., 1969, Petroleum potential of the Kandik basin, east-central Alaska: *USGS Open-File Report,* 1305, 11 pp.

Dembicki, H., Jr., 1984, An interlaboratory comparison of source rock data: *Geochim. et Cosmochim. Acta*, v. 48, p. 2641-2649.

Dorsey, R.J., Buchovecky, E.J., and Lundberg, N., 1988, Clay mineralogy of Pliocene-Pleistocene mudstones, eastern Taiwan: Combined effects of burial diagenesis and provenance unroofing: *Geology*, v. 16, p. 944-947.

Dover, J.H., 1985, Possible oroclinal bend in northern Cordilleran fold and thrust belt, east-central Alaska: *GSA Abst. w. Prog.*, v. 17, p. 352.

Dover, J.H., and Miyaoka, R.T., 1988, Reinterpreted geologic map and fossil data, Charley River Quadrangle, east-central Alaska: *USGS Misc. Field Studies Map*, MF-2004, scale 1:250,000.

Dow, W.G., 1977, Kerogen studies and geological interpretations: *Jour. of Geochem. Explor.*, v. 7, p. 79-99.

Dow, W.G., and O'Connor, D.E., 1982, Kerogen maturity and type by reflected light microscopy applied to petroleum generation, in *How to assess maturation and paleotemperatures*: SEPM Short Course 7, p. 133-157.

Duba, D., and Williams-Jones, A.E., 1983, The application of illite crystallinity, organic matter reflectance, and isotopic techniques to mineral exploration: A case study in southwestern Gaspe, Quebec: *Econ. Geol.*, v. 78, p. 1350-1363.

Dunoyer de Segonzac, G., 1970, The transformation of clay minerals during diagenesis and low-grade metamorphism: A review: *Sedimentology*, v. 15, p. 281-346.

Espitalie, J., Madec, M., Tissot, B., Menning, J.J., and Leplat, P., 1977, Source rock characterization method for petroleum exploration: *Proc. of the 9th Annual Offshore Tech. Conf.*, v. 3, p. 439-448.

Espitalie, J., Madec, M., and Tissot, B., 1980, Role of mineral matrix inkerogen pyrolysis; influence on petroleum generation and migration: *AAPG Bulletin*, v. 64, p. 59-66.

Foster, H.L., 1976, Geologic map of the Eagle Quadrangle, Alaska: *USGS Misc. Invest. Map*, I-922, scale 1:250,000.

Frey, M., Teichmuller, M., Teichmuller, R., Mullis, J., Kunzi, B., Breitschmid, A., Gruner, U., and Schwizer, B., 1980, Very low-grade metamorphism in external parts of the Central Alps: Illite crystallinity, coal rank and fluid inclusion data: *Ecolgae geol. Helv.*, v. 73, p. 173-203.

Furlong, K.P., and Edman, J.D., 1984, Graphic approach to determination of hydrocarbon maturation in overthrust terrains: *AAPG Bulletin*, v. 68, p. 1818-1824.

Gaudette, H.E., Eades, J.L., and Grim, R.E., 1966, The nature of illite: *Clays and Clay Min.*, v. 13, p. 33-48.

Green, L.H., and Roddick, J.A., 1961, Geology, Dawson, Yukon Territory: *Geol. Survey Canada Map* 1284-A.

Guthrie, J.M., Houseknecht, D.W., and Johns, W.D., 1986, Relationships among vitrinite reflectance, illite crystallinity, and organic geochemistry in Craboniferous strata, Ouachita Mountains, Oklahoma and Arkansas: *AAPG Bulletin*, v. 70, p. 26-33.

Hood, A., Gutjahr, C.C.M., and Heacock, R.L., 1975, Organic metamorphism and the generation of petroleum: *AAPG Bulletin*, v. 59, p. 986-996.

Howell, D.G., and Wiley, T.J., 1987, Crustal evolution of northern Alaska inferred from sedimentology and structural relations of the Kandik area: *Tectonics*, v. 6, p. 619-631.

Hower, J., Eslinger, W.V., Hower, M., and Perry, E.A., 1976, Mechanisms of burial metamorphism of argillaceous sediments, I. Mineralogical and chemical evidence: *GSA Bulletin*, v. 87, p. 725-737.

Hower, J.C., and Davis, A., 1981, Vitrinite reflectance anisotropy as a tectonic fabric element: *Geology*, v. 9, p. 165-168.

Katz, B.J., 1983, Limitations of "Rock-Eval" pyrolysis for typing organic matter: *Organic Geochemistry*, v. 4, p. 195-199.

Kisch, H.J., 1980, Illite crystallinity and coal rank associated with lowest-grade metamorphism of the Taveyanne graywacke in the Helvetic zone of the Swiss Alps: *Ecolgae Geol. Helv.*, v. 73, p. 753-777.

Kisch, H.J., 1987, Correlation between indicators of very low-grade metamorphism, in M. Frey, ed., *Low Temperature Metamorphism*: New York, Chapman and Hall, p. 227-346.

Kubler, B., 1968, Evaluation quantitative du metamorphisme par la cristallinite de l'illite: *Societe Nationale des Petroles d'Aquitaine Centre de Recherches Bulletin*, v. 2, p. 385-397.

Levine, J.R., and Davis, A., 1984, Optical anisotropy of coals as an indicator of tectonic deformation, Broad Top Coal Field, Pennsylvania: *GSA Bulletin*, v. 95, p. 100-108.

Norris, D.K., 1979, Geology, Ogilvie River, Yukon Territory: *Geol. Survey Canada Map*, 1526-A.

Peters, K.E., 1986, Guidelines for evaluating petroleum source rocks using programmed pyrolysis: *AAPG Bulletin*, v. 70, p. 318-329.

Perry, E., and Hower, J., 1970, Burial diagenesis in Gulf Coast pelitic sediments: *Clay and Clay Min.*, v. 18, p. 165-177.

Price, L.C., 1983, Geologic time as a parameter in organic metamorphism and vitrinite reflectance as an absolute paleogeothermometer: *Jour. of Petroleum Geol.*, v. 6, p. 5-38.

Price, L.C., and Barker, C.E., 1985, Suppression of vitrinite reflectance in amorphous rich kerogen - a major unrecognized problem: *Jour. of Petroleum Geol.*, v. 8, p. 59-84.

Reynolds, R.C., and Hower, J., 1970, The nature of interlayering in mixed-layer illite-montmorillinites: *Clays and Clay Min.*, v. 18, p. 25-36.

Stach, E., Mackowsky, M-Th., Teichmuller, M., Taylor, G.H., Chandra, D., and Teichmuller, R., 1982, *Stach's Textbook of Coal Petrology*: Berlin, Gerbruder Borntraeger, 511 pp.

Stone, I.J., and Cook, A.C., 1979, The influence of some tectonic structures upon vitrinite reflectance: *Jour. of Geol.*, v. 87, p. 497-508.

Underwood, M.B., 1989, Temporal changes in geothermal gradient, Franciscan subduction complex, northern California: *Jour. of Geophys. Res.*, v. 94, p. 3111-3125.

Underwood, M.B., and O'Leary, J.D., 1985, Vitrinite reflectance and paleotemperature within Franciscan terranes of coastal northern California: 38°45'N to 40°00'N: *USGS Open-File Report*, 85-663, 32 pp.

Underwood, M.B., and Strong, R.H., 1986a, Vitrinite reflectance and estimates of paleotemperature for Franciscan terranes of northern California: 40°00'N to 40°35'N: *USGS Open-File Report* , 86-258, 41 pp.

Underwood, M.B., and Strong, R.H., 1986b, Vitrinite reflectance and illite crystallinity, Cambria slab and Franciscan Complex, central California coast: *USGS Open-File Report,* 86-295, 19 pp.

Waples, D.W., 1980 Time and temperature in petroleum formation: Application of Lopatin's method to petroleum exploration: *AAPG Bulletin*, v. 64, p. 916-926.

APPENDIX A. HISTOGRAMS OF VITRINITE REFLECTANCE DATA KANDIK BASIN, ALASKA

Key to Symbols

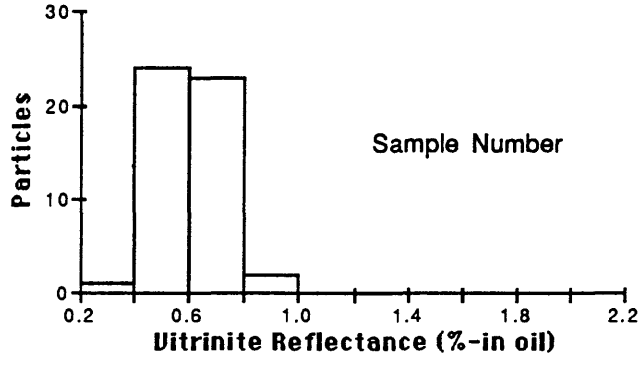

Devonian strata

Triassic- Cretaceous (Glenn Shale)

Cretaceous (Kandik Group)

data omitted from calculations of mean

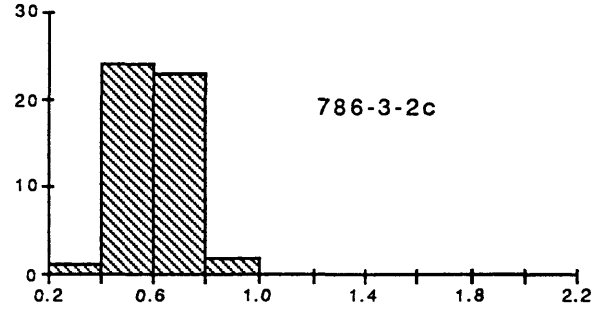
786-3-2c
30
20
10
0
0.2
0.6
1.0
1.4
1.8
2.2

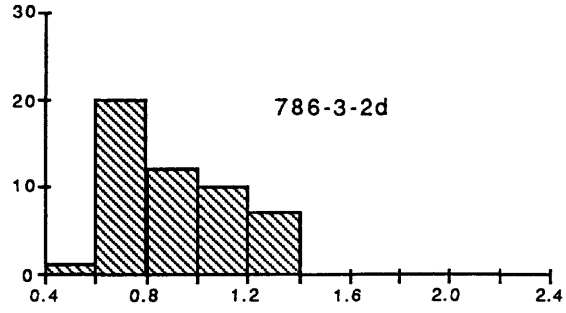
786-3-2d
30
20
10
0
0.4
0.8
1.2
1.6
2.0
2.4

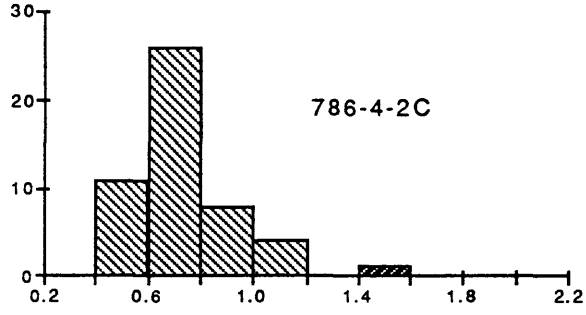
786-4-2C
30
20
10
0
0.2
0.6
1.0
1.4
1.8
2.2

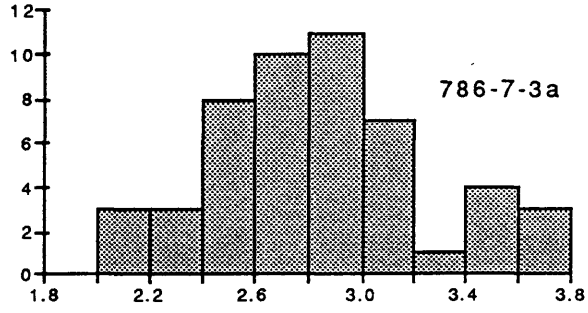
786-7-3a
12
10
8
6
4
2
0
1.8
2.2
2.6
3.0
3.4
3.8

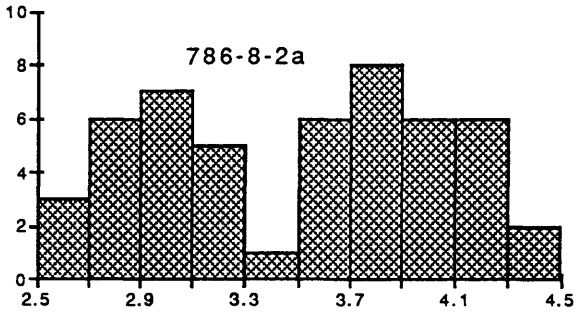
786-8-2a
10
8
6
4
2
0
2.5
2.9
3.3
3.7
4.1
4.5

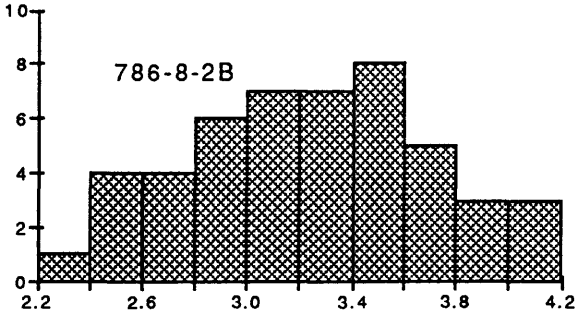
786-8-2B
10
8
6
4
2
0
2.2
2.6
3.0
3.4
3.8
4.2

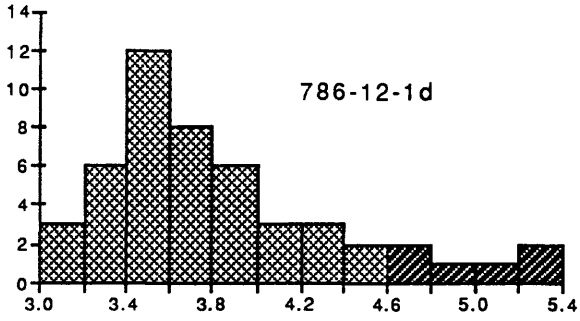
786-12-1d
14
12
10
8
6
4
2
0
3.0
3.4
3.8
4.2
4.6
5.0
5.4

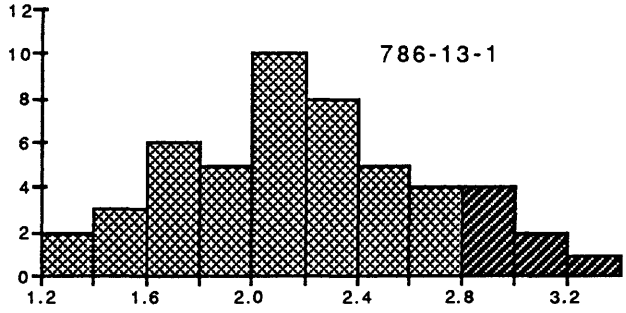
786-13-1
12
10
8
6
4
2
0
1.2
1.6
2.0
2.4
2.8
3.2

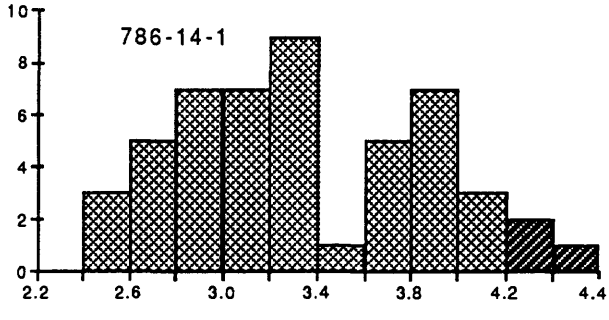
786-14-1
10
8
6
4
2
0
2.2
2.6
3.0
3.4
3.8
4.2
4.4

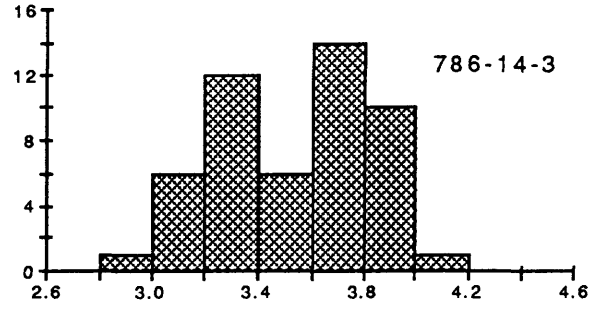
786-14-3
16
12
8
4
0
2.6
3.0
3.4
3.8
4.2
4.6

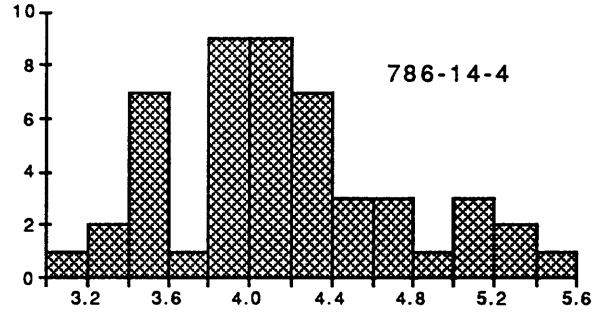
786-14-4
10
8
6
4
2
0
3.2
3.6
4.0
4.4
4.8
5.2
5.6

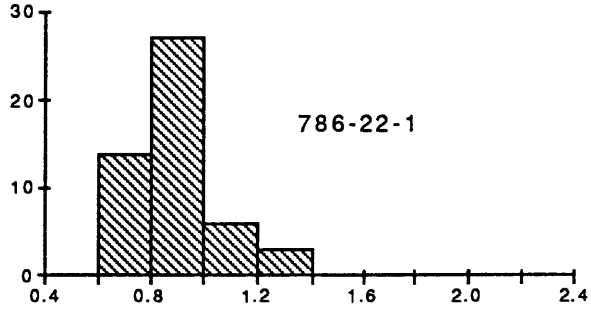
786-22-1
30
20
10
0
0.4
0.8
1.2
1.6
2.0
2.4

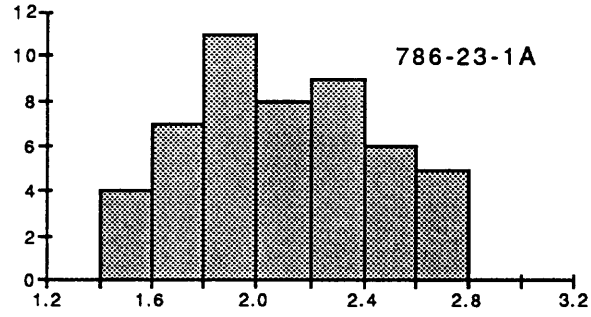
786-23-1A
12
10
8
6
4
2
0
1.2
1.6
2.0
2.4
2.8
3.2

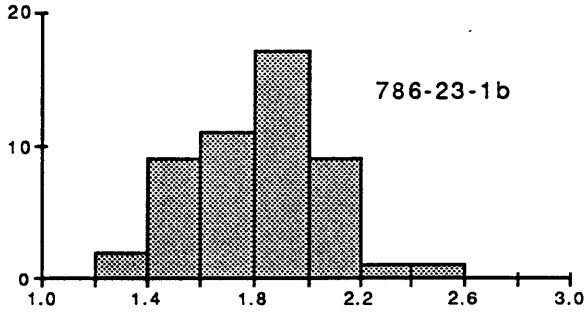
786-23-1b
20
10
0
1.0
1.4
1.8
2.2
2.6
3.0

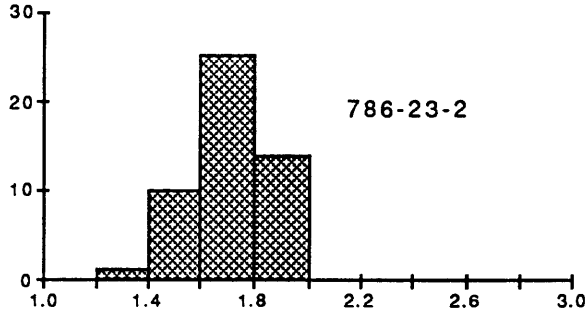
786-23-2
30
20
10
0
1.0
1.4
1.8
2.2
2.6
3.0

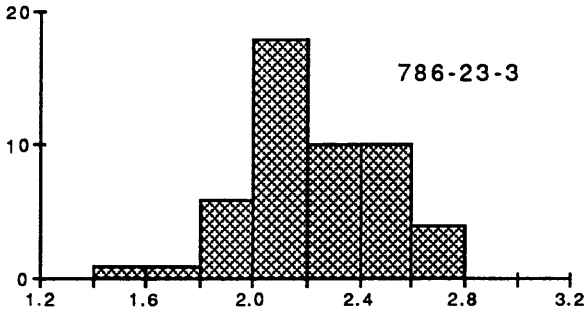
786-23-3
20
10
0
1.2
1.6
2.0
2.4
2.8
3.2

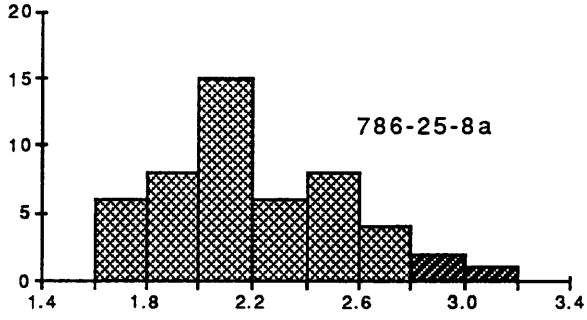
786-25-8a
20
15
10
5
0
1.4
1.8
2.2
2.6
3.0
3.4

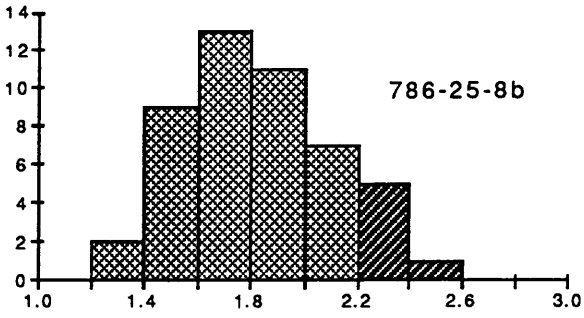
786-25-8b
14
12
10
8
6
4
2
0
1.0
1.4
1.8
2.2
2.6
3.0

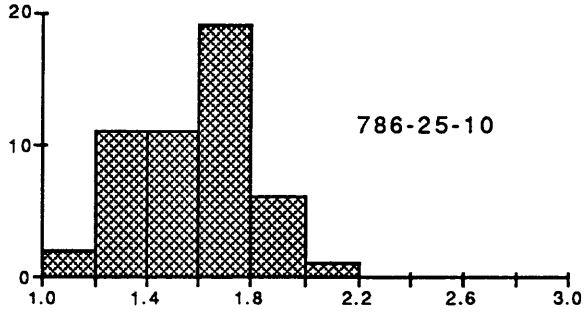
786-25-10
20
10
0
1.0
1.4
1.8
2.2
2.6
3.0

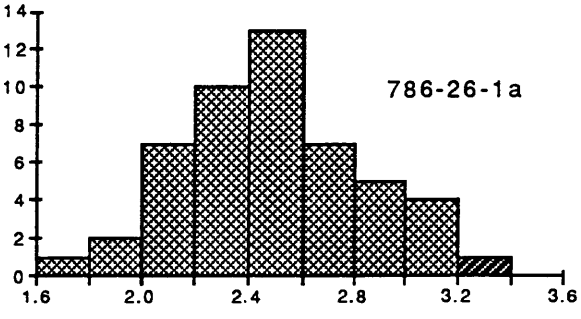
786-26-1a
14
12
10
8
6
4
2
0
1.6
2.0
2.4
2.8
3.2
3.6

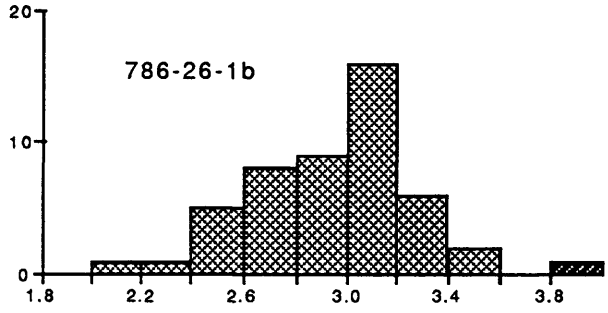
786-26-1b
20
10
0
1.8
2.2
2.6
3.0
3.4
3.8

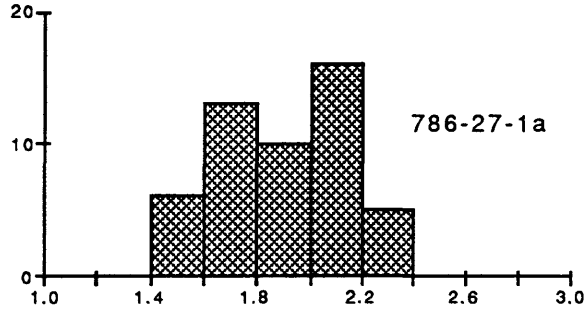
786-27-1a
20
10
0
1.0
1.4
1.8
2.2
2.6
3.0

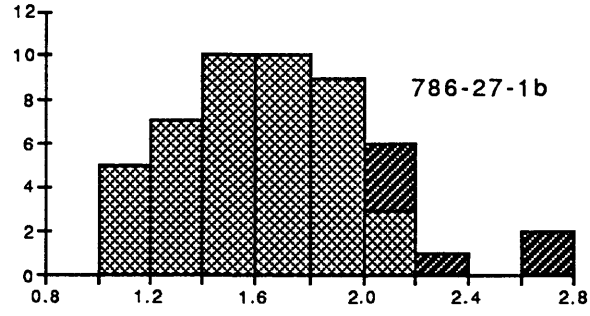
786-27-1b
12
10
8
6
4
2
0
0.8
1.2
1.6
2.0
2.4
2.8

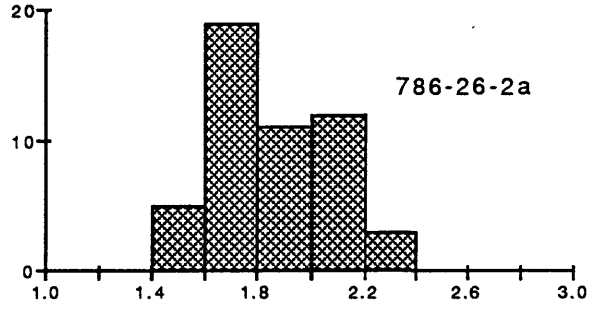
786-26-2a
20
10
0
1.0
1.4
1.8
2.2
2.6
3.0

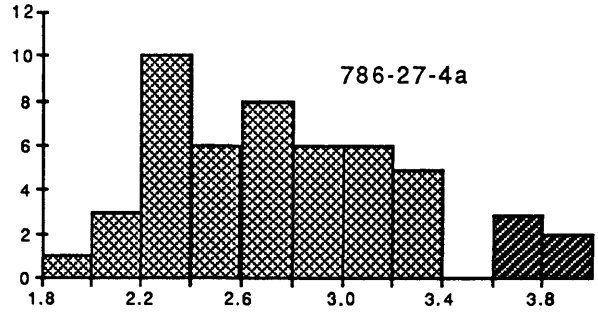
786-27-4a
12
10
8
6
4
2
0
1.8
2.2
2.6
3.0
3.4
3.8

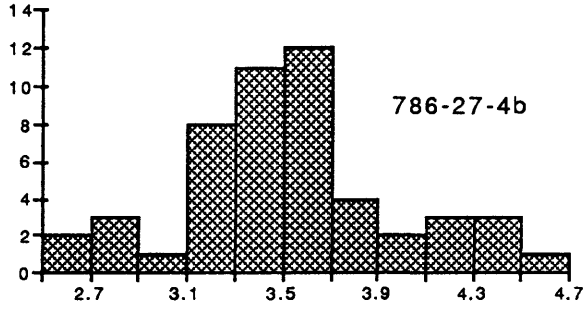
786-27-4b
14
12
10
8
6
4
2
0
2.7
3.1
3.5
3.9
4.3
4.7

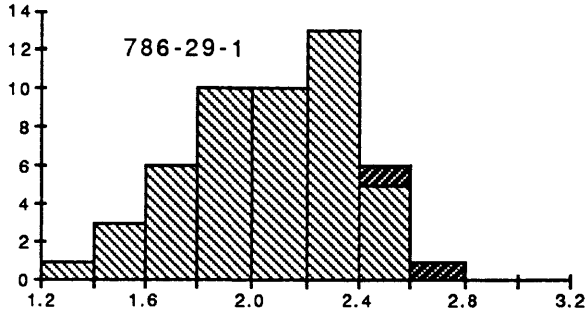
786-29-1
14
12
10
8
6
4
2
0
1.2
1.6
2.0
2.4
2.8
3.2

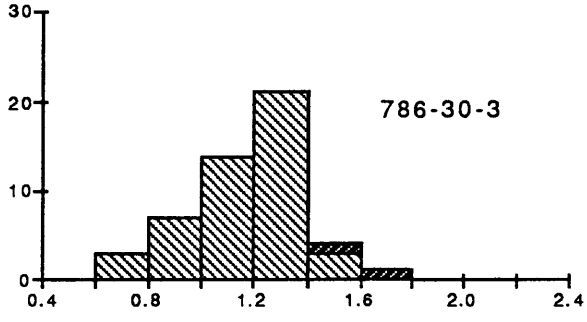
786-30-3
30
20
10
0
0.4
0.8
1.2
1.6
2.0
2.4

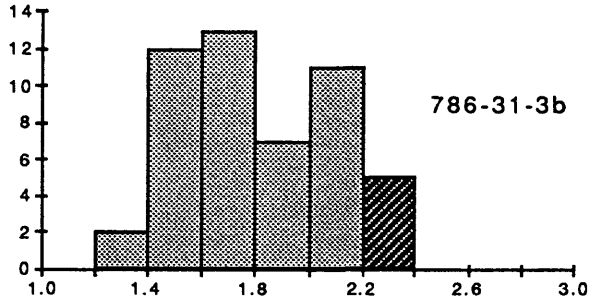
786-31-3b
14
12
10
8
6
4
2
0
1.0
1.4
1.8
2.2
2.6
3.0

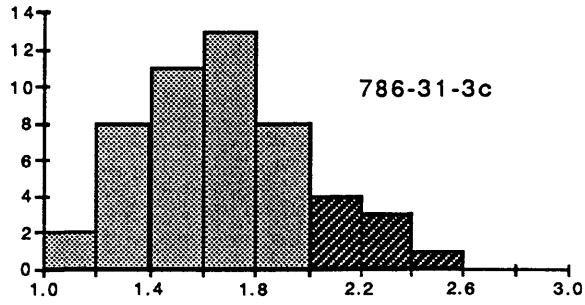
786-31-3c
14
12
10
8
6
4
2
0
1.0
1.4
1.8
2.2
2.6
3.0

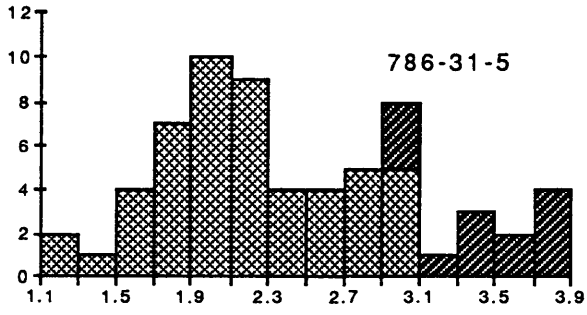
786-31-5
12
10
8
6
4
2
0
1.1
1.5
1.9
2.3
2.7
3.1
3.5
3.9

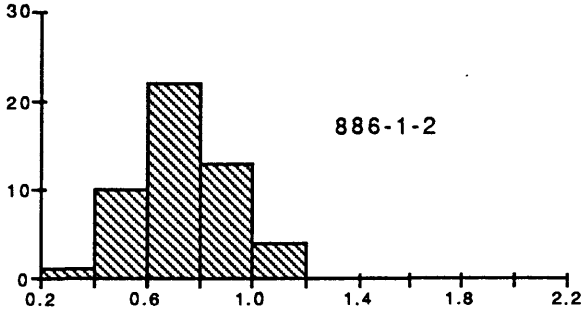
886-1-2
30
20
10
0
0.2
0.6
1.0
1.4
1.8
2.2

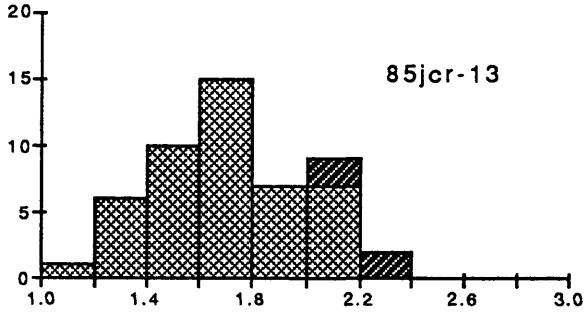
85jcr-13
20
15
10
5
0
1.0
1.4
1.8
2.2
2.6
3.0

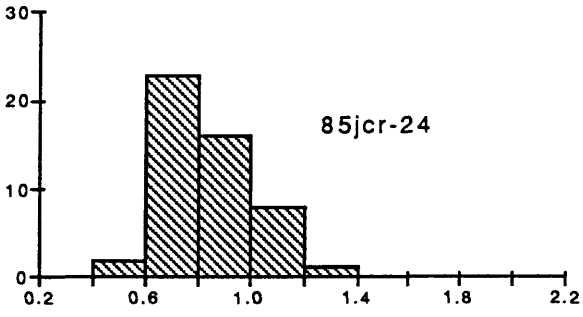
85jcr-24
30
20
10
0
0.2
0.6
1.0
1.4
1.8
2.2

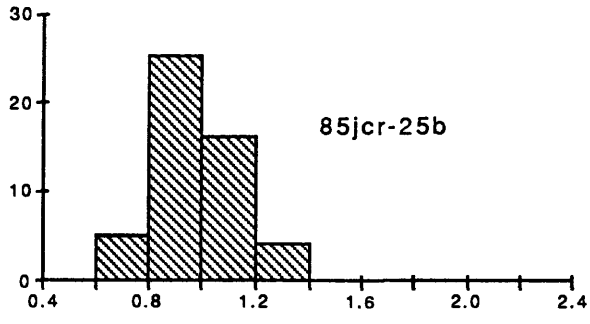
85jcr-25b
30
20
10
0
0.4
0.8
1.2
1.6
2.0
2.4

APPENDIX B. THERMAL-MATURITY DATA, KANDIK BASIN, ALASKA

Sample Number	Fault Block	Rock Unit	Mean Ro (%)	No.	Range	Stan. Dev.	Ill. Xtl. ($\Delta°2\theta$)
786-3-2c	NR	Dnr	0.61	50	0.39-0.96	0.11	
786-3-2d	NR	Dnr	0.90	50	0.59-1.31	0.22	0.52
786-3-3a	NR	Dnr					0.53
786-4-2c	NR	Dnr	0.71	49	0.44-1.08	0.15	0.51
786-7-2	NR	pCt					0.33
786-7-3a	KR	KTrg	2.83	50	2.00-3.70	0.40	0.33
786-7-3b	KR	KTrg					0.39
786-8-2a	KR	Kb	3.49	50	2.50-4.42	0.54	
786-8-2b	KR	Kb	3.29	50	2.25-4.27	0.50	0.31
786-12-1d	KR	Kb	3.67	43	3.10-4.49	0.35	0.28
786-13-1	KR	Kb	2.09	43	1.20-2.78	0.38	0.41
786-14-1	KR	Kb	3.27	47	2.42-4.09	0.48	0.31
786-14-3	KR	Kb	3.55	50	2.99-4.01	0.29	0.32
786-14-4	KR	Kb	4.16	49	3.09-5.48	0.57	0.35
786-22-1	NR	Dm	0.89	50	0.62-1.34	0.15	
786-23-1a	KR	KTrg	2.10	50	1.45-2.73	0.35	0.58
786-23-1b	KR	KTrg	1.82	50	1.29-2.40	0.25	0.62
786-23-2	KR	Kb	1.70	50	1.30-1.89	0.13	0.50
786-23-3	KR	Kb	2.21	50	1.55-2.72	0.26	0.58
786-24-1b	KR	Kka					0.44
786-24-2b	KR	Kka					0.46
786-24-3a	KR	Kka					0.37
786-24-3b	KR	Kka					0.40
786-25-8a	KR	Kka	2.17	47	1.60-2.77	0.30	0.47
786-25-8b	KR	Kka	1.75	42	0.58-2.12	0.23	0.42
786-25-10	KR	Kka	1.58	50	1.17-2.05	0.22	0.37
786-26-1a	KR	Kkg	2.48	49	1.76-3.09	0.33	
786-26-1b	KR	Kkg	2.94	48	2.12-3.56	0.31	0.55
786-26-3a	KR	Kka					0.48
786-26-3b	KR	Kka					
786-27-1a	KR	Kb	1.90	50	1.43-2.37	0.24	0.39
786-27-1b	KR	Kb	1.58	44	1.05-2.08	0.28	0.50
786-27-2a	KR	Kb	1.85	50	1.51-2.29	0.21	
786-27-2b	KR	Kb					
786-27-4a	KR	Kb	2.68	45	1.94-3.32	0.38	0.37
786-27-4b	KR	Kb	3.52	50	2.55-4.61	0.46	0.32
786-29-1	NR	Dnr	2.04	48	1.35-2.49	0.29	0.57
786-30-3	NR	Dm	1.13	48	0.60-1.41	0.19	
786-30-4	NR	Dm					
786-30-5	NR	unkn					0.50
786-31-3a	KR	KTrg					0.78
786-31-3b	KR	KTrg	1.76	45	1.35-2.19	0.24	0.74

Appendix B. (continued)

Sample Number	Fault Block	Rock Unit	Mean Ro (%)	No.	Range	Stan. Dev.	Ill. Xtl. (Δ°2θ)
786-31-3c	KR	KTrg	1.57	42	1.11-1.98	0.22	0.83
786-31-5	KR	Kkg	2.09	46	1.13-2.95	0.41	
886-1-1	NR	Ch					0.54
886-1-2	NR	DOSr	0.72	50	0.39-1.02	0.16	
85jcr-11	KR	MDf					0.37
85jcr-13	KR	Kka	1.67	46	1.19-2.09	0.24	
85jcr-14	KR	Kka					0.54
85jcr-15a	NR	Dnr					0.67
85jcr-24	NR	Dnr	0.82	50	0.55-1.22	0.16	0.59
85jcr-25b	NR	DOSr	0.97	50	0.72-1.33	0.15	0.53
85jcr-67	NR	pCt					0.43

APPENDIX C. DATA FROM ROCK-EVAL PYROLYSIS, KANDIK BASIN, ALASKA

Sample Number	Rock Unit	TOC (wt-%)	TMAX[1] (°C)	2 HI	3 OI	4 PI
786-3-2c	Dnr	0.40	443	42	95	0
786-3-2d	Dnr	0.40	446	65	80	0.11
786-3-3a	Dnr	0.30	449	43	100	0
786-4-2c	Dnr	0.35	429	45	111	0.05
786-7-2	pCt	0.57		14	107	0.12
786-7-3a	KTrg	1.79		3	56	0.17
786-7-3b	KTrg	0.44		4	115	0
786-8-2a	Kb	1.28		4	42	0.17
786-8-2b	Kb	0.82		4	56	0
786-12-1d	Kb	0.78		5	10	0.25
786-13-1	Kb	0.88		6	20	0.17
786-14-1	Kb	1.00		1	20	0
786-14-3	Kb	1.12		0	15	0
786-14-4	Kb	1.00		0	29	0
786-22-1	Dm	1.73	447	242	24	0.05
786-23-1a	KTrg	1.16	503	2	37	0
786-23-1b	KTrg	1.47	568	4	33	0.25
786-23-2	Kb	0.62		16	43	0.25
786-23-3	Kb	1.17	579	5	21	0
786-24-1b	Kka	0.63		11	20	0.12
786-24-2b	Kka	0.40		5	20	0
786-24-3a	Kka	0.30		23	50	0.12
786-24-3b	Kka	0.37		8	37	0
786-25-8a	Kka	0.60	460	3	18	0
786-25-8b	Kka	0.75	475	13	30	0.1
786-25-10	Kka	1.21	560	8	13	0.1
786-26-1a	Kkg	0.52		13	44	0.25
786-26-1b	Kkg	0.93	450	2	29	0
786-26-3a	Kka	0.20		0	50	0
786-26-3b	Kka	0.15		26	60	0
786-27-1a	Kb	0.95		7	6	0
786-27-1b	Kb	0.93		1	16	0
786-27-2a	Kb	0.37		10	81	0.25
786-27-2b	Kb	0.62		4	59	0.25
786-27-4a	Kb	0.95		0	37	0
786-27-4b	Kb	0.61		0	21	0
786-29-1	Dnr	0.41		12	87	0.17
786-30-3	Dm	5.26	473	77	7	0.07
786-30-4	Dm	1.75	472	45	17	0.1

Appendix C. Continued

Sample Number	Rock Unit	TOC (wt-%)	TMAX[1] (°C)	HI[2]	OI[3]	PI[4]
786-31-3a	KTrg	1.60	572	9	16	0.22
786-31-3b	KTrg	1.75	555	8	14	0.25
786-31-3c	KTrg	1.61	543	3	12	0.17
786-31-5	Kkg	0.69		0	50	0
886-1-1	Ch	1.49	433	167	18	0.11
886-1-2	DSOr	1.80	442	169	27	0.11

[1] TMAX values greater than 580°C were not recorded
[2] HI = hydrogen index (*mg* HC/*g* TOC)
[3] OI = oxygen index (*mg* CO_2/*g* TOC)
[4] PI = production index [S1+(S1+S2)]